The Impact of Oxygen Depletion and the Concomitant Acidification of Bottom Waters on the Preservation of Detrital Carbonates in the Gulf of St. Lawrence

By

William Alexander Selkirk Nesbitt

Department of Earth and Planetary Sciences

McGill University

Montréal, QC, Canada

December 2018

A thesis submitted to McGill University in partial fulfillment of the requirements of the degree of Master of Science

Table of Contents

Abstract

Over the past century, dissolved oxygen concentrations (DO) in the bottom waters of the Lower St. Lawrence Estuary (LSLE) and the Gulf have decreased dramatically and led to the development of persistent hypoxia ($[O_2]$ = <62.5μmol/L) in the LSLE. Oxygen depletion has been attributed primarily to changes in ocean circulation in the northwest Atlantic Ocean and an increase in the flux of organic matter to the seafloor. Accumulation of metabolic CO_2 in these waters has also resulted in their acidification and a decrease in pH (0.3-0.4 pH unit), commensurate to the variation expected for oceanic surface waters by the end of this century, thus, making this setting an excellent analogue for studies of ocean acidification and its potential ecological impacts. The decrease in bottom-water pH is accompanied by a decrease in the carbonate ion concentration and the saturation state of the waters with respect to both calcite and aragonite (Ω_C and Ω_A). Although the Laurentian Trough sediments are mostly devoid of modern calcium carbonate fossils, detrital (Ordovician/Silurian) carbonates originating from Anticosti Island accumulate on the neighboring seafloor. Whereas aragonite is absent in these sediments, to the best of our knowledge the preservation and dissolution of calcite has not been documented. This study examines the impact of oxygen depletion and the concomitant acidification of bottom waters on the preservation of these detrital carbonates in the Laurentian Trough sediments. Evidence of carbonate mineral dissolution is presented through an analysis of the inorganic carbon content of the sediments and their pore water composition. Historical data are used to determine the temporal evolution of the solid phase profiles as well as document the differential spatial preservation of the detrital carbonates. Finally, the mineralogy, chemical (Mg/Ca) and stable isotopic composition ($\delta^{13}C$ and $\delta^{18}O$) of the carbonates in sediment cores recovered in the Trough were compared to the source material eroded from Anticosti Island.

Résumé

Au cours du siècle dernier, les concentrations en oxygène dissous dans les eaux profondes de l'estuaire maritime du Saint-Laurent (EMSL) et du Golfe ont diminuées dramatiquement, menant à une hypoxie persistante ([O_2] = <62.5µmol/L). L'appauvrissement en oxygène dissous est principalement due aux changements de la circulation océanique dans le nord-ouest Atlantique et à une augmentation du flux de matière organique vers le fond. L'accumulation de CO_2 métabolique dans ces eaux résulte en leur acidification et à une chute du pH (de 0.3-0.4 unité de pH), semblable aux variations attendues pour les eaux océaniques de surface d'ici la fin du siècle. Ainsi, cet environnement est un excellent analogue pour l'étude de l'acidification des océans et ses impacts écologiques potentiels. La diminution du pH des eaux profondes est accompagnée par une diminution de la concentration des ions carbonates et de l'état de saturation de l'eau par rapport à la calcite et à l'aragonite (Ω_C and Ω_A). Alors que les sédiments de la fosse laurentienne ne contiennent généralement pas de fossiles modernes de carbonate de calcium, des carbonates détritiques (Ordovicien/Silurien) provenant de l'île d'Anticosti s'accumulent sur le fond marin avoisinant. Quoique ces sédiments ne contiennent pas d'aragonite, au meilleur de notre connaissance, la préservation et la dissolution de la calcite n'a pas été documentée. Cette étude examine les impacts de la diminution en oxygène dissous et de l'acidification concomitante sur la préservation de ces carbonates détritiques dans les sédiments de la fosse laurentienne. Nous documentons la dissolution des minéraux carbonatés à l'aide d'une analyse du contenu en carbone inorganique des sédiments et de la composition de leurs eaux porales. Des données historiques sont utilisées pour déterminer l'évolution temporelle des profils de la phase solide ainsi que documenter la variabilité spatiale de la préservation. Finalement, nous comparons la composition minéralogique, chimique (Mg/Ca) et isotopique ($\delta^{13}C$ and $\delta^{18}O$) des carbonates de carottes de sédiment provenant de la fosse et du matériel source érodé de l'île d'Anticosti.

List of Figures

List of Tables

Acknowledgements

The past two years were full of challenges and triumphs, ultimately leading to a rewarding M.Sc. experience. None of this, however, would have been possible without the people who stood by me during this adventure.

Firstly, I would like to thank my thesis supervisor, Dr. Alfonso Mucci, and the Department of Earth and Planetary Science for academic and financial support. Working with Al was not just an opportunity, but a pleasure. His guidance, patience, thorough editing, and contagious enthusiasm for science were integral in my growth as a scientist over these past couple of years. Al taught me to be critical, rigorous and concise in my research, which greatly contributed to the completion of this thesis. I would also like to thank Al for the opportunity to present my work at the 2018 Ocean Sciences Meeting (OSM) in Portland, Oregon.

I would like to acknowledge Dr. Galen Halverson for his invaluable input as a member of my thesis committee and to extend my gratitude to Constance Guignard for her technical support and time in the laboratory. I am extremely grateful to the Captains and crew of the R/V Coriolis II, for this project would not have been possible without their dedication.

I would like to thank the other members of the lab – Olivier, Louise, Alexis, Ashley, Mathilde and Pascale – for their encouragement, input and friendship. I would also like to express my gratitude to the others I shared an office with in 131A – Becky and Longbo – and the rest of my friends in Montreal who made my time here fun and memorable.

I would like to extend special thanks to my family – Mom, Dad, Liz, Richard, Vic, Ryan, and Angus – you guys have been there with me every step of the way and never stopped believing in me. Finally, I would like to thank my partner-in-crime, Shelby, you've been there with me through good and bad times and I would not be where I am today without you.

Author Contributions

The results and interpretations of this thesis are presented in the form of a co-authored paper. The two authors of the paper are William Nesbitt and Alfonso Mucci. Analysis of data, calculations, interpretations and writing were done by William Nesbitt. Alfonso Mucci contributed historical data sets, supervision, editing and funding to this research.

Chapter 1: Introduction

1.1 - Ocean Acidification

1.11 - Climate change and atmospheric CO_2

Over the past 180 years, global anthropogenic carbon dioxide (CO_2) emissions have increased exponentially in response to the progressive use of fossil fuels, deforestation and land use changes (Feely et al., 2004; Doney et al., 2009; Feely et al., 2009). This has caused atmospheric CO_2 levels to surpass the 400 ppm mark at the end of 2014, exceeding pre-industrial concentrations by nearly 40%, and reaching levels higher than any recorded in the past 800,000 years (Feely et al., 2004; Sabine and Feely, 2007; Doney et al., 2009; Feely et al., 2009; Le Quéré et al., 2009; Tans and Keeling, 2016). This has had impacts across the globe such as rising average temperatures, decreasing sea-ice cover at the poles and ocean acidification (IPCC, 2007).

Atmospheric CO_2 concentrations are expected to rise at an even faster pace in the coming decades due to an ever-growing population, which is projected to exceed 11 billion people by 2100 (United Nations, 2017). This considerable increase, from the current population of 7.4 billion, will bring about a surge in the demand for energy, food, and land. The Intergovernmental Panel on Climate Change (IPCC) developed a series of projections for future atmospheric CO_2 concentrations that range from the current rate of emissions to increases matching the population growth. A newer projection, following the 2015 Paris Climate Accord, suggests that if every country that signed the accord were to abide to their pledges, atmospheric CO_2 concentrations will reach 670 ppm by the end of this century. More realistic predictions such as the "business-as-usual" scenario (IS92a), however, foresee CO_2 concentrations exceeding 700 ppm by the end of this century.

1.12 - CO_2 uptake by the surface ocean

Since the beginning of the industrial revolution, the ocean, the largest CO_2 reservoir and sink on Earth, has taken up just over a quarter of all anthropogenic CO_2 emissions to the atmosphere (Feely et al., 2004; Sabine and Feely, 2007; Feely et al., 2009; Gattuso and Hansson, 2011). The sequestration of atmospheric CO_2 by the oceans has greatly curbed the effects of climate change and the visible impacts of global warming, but it does not do so without consequences as it leads to ocean acidification, i.e., a decrease in the pH of seawater (Doney et al., 2009; Feely et al., 2009). Ocean acidification can have deleterious effects on marine ecosystems, especially to organisms that secrete calcium carbonate shells and skeletons as it makes calcification more difficult. Additionally, non-calcifying organisms may suffer physiological impairments (e.g., growth rate, reproduction), due to a drop in pH as CO_2 reacts with body fluids, causing changes to their metabolic rates (Fabry et al., 2008; Miller et al., 2009; Ries et al., 2009; Kroecker et al., 2013).

The interaction between atmospheric CO_2 and the surface ocean can be readily described by reactions of the CO_2-seawater system. When CO_2 dissolves in seawater and enters the aqueous phase as $CO_{2(aq)}$, a portion of the solvated CO_2 is converted to carbonic acid (H_2CO_3) (Morse et al., 2007; Gattuso and Hansson, 2011: see Equation 1). The relationship between atmospheric and oceanic CO_2 concentrations is described by Henry's Law (see Equation 2), where the equilibrium concentration of $CO_{2(aq)}$ is given by the product of the partial pressure of $CO_{2(gas)}$ (pCO_2) in the gas phase (atmosphere) and its solubility product in seawater (K^*_H) (Gattuso and Hansson, 2011).

$$CO_2 + H_2O \rightleftharpoons H_2CO_3^* \quad \textbf{(1)}$$

$$[H_2CO_3^*] = pCO_2 * K_H^* \quad \textbf{(2)}$$

$H_2CO_3^*$ is commonly used to describe the sum of carbonic acid and $CO_{2(aq)}$ because it is difficult to distinguish them analytically within a solution. True H_2CO_3 typically only accounts for ~0.3% of $H_2CO_3^*$ (Millero et al., 2002; Morse et al., 2007; Gattuso and Hansson, 2011).

H_2CO_3 is a weak acid and subsequently undergoes partial dissociation, leading to an increase in the effective concentration of protons (H^+) and a decrease in pH (pH = -log(H^+)) of the solution (Millero et al., 2002; Morse et al., 2007; Gattuso and Hansson, 2011: see Equations 3 and 4).

$$H_2CO_3^* \rightleftharpoons HCO_3^- + H^+ \quad \textbf{(3)}$$

$$HCO_3^- \rightleftharpoons CO_3^{2-} + H^+ \quad \textbf{(4)}$$

The reactions within the CO_2-seawater system are fully reversible, meaning that the carbonate ion (CO_3^{2-}), if present in seawater, can neutralize protons (H^+) released upon the dissociation of $H_2CO_3^*$ and buffers the pH change in response to ocean acidification (Millero et al., 2002).

The two dissociation reactions, as described in Equations 3 and 4 above, are governed by the stoichiometric equilibrium constants K_1^* and K_2^* respectively (see Equations 5 and 6). These constants are defined by the ratio of the concentration of the products over the reactants of the reactions. Since they are defined in terms of concentrations instead of activities, these constants vary with temperature, pressure and salinity. Their absolute values also depend on the thermodynamic convention and pH scale used to define the activity or concentration of the proton (Dickson, 1984). Hence, the inorganic carbon speciation is strongly dependent on pH.

$$K_1^* = \frac{[HCO_3^-][H^+]}{[H_2CO_3^*]} \quad \textbf{(5)}$$

$$K_2^* = \frac{[CO_3^{2-}][H^+]}{[HCO_3^-]} \quad \textbf{(6)}$$

Using the K_1^* and K_2^* values, the speciation of the dissolved inorganic carbon (DIC = $[H_2CO_3^*] + [HCO_3^-] + [CO_3^{2-}]$) can be calculated for a set of environmental conditions at any given pH according to:

$$[H_2CO_3^*] = \frac{[H^+]^2}{[H^+]^2 + K_1^*[H^+] + K_1^*K_2^*} * [DIC] \quad \textbf{(7)}$$

$$[HCO_3^-] = \frac{K_1^*[H^+]}{[H^+]^2 + K_1^*[H^+] + K_1^*K_2^*} * [DIC] \quad \textbf{(8)}$$

$$[CO_3^{2-}] = \frac{K_1^* K_2^*}{[H^+]^2 + K_1^*[H^+] + K_1^* K_2^*} * [DIC] \quad \textbf{(9)}$$

These concentrations can be plotted on a Bjerrum or speciation diagram as a function of pH (Wolf-Gladrow et al., 2007; see Figure 1.1). At the pH of the surface ocean ($pH_T \approx 8.1$, total proton concentration scale defined under the constant ionic medium convention), most of the DIC is present as HCO_3^- (90%), approximately 9% is in the form of CO_3^{2-} and only 1% as $H_2CO_3^*$ (or $CO_{(aq)}$) (Orr et al., 2005; Doney et al., 2009; Gattuso and Hansson, 2011).

Over the last century, uptake of CO_2 from the atmosphere has decreased the pH of the ocean surface by an estimated 0.1 unit, equivalent to a 30% increase in the proton concentration in solution (Caldeira and Wickett, 2005). If projected atmospheric CO_2 concentrations for the end of this century are accurate (~700 ppm) and the pH of the surface ocean falls by an additional ~0.4 unit, this will dramatically affect the speciation of DIC in seawater (see Figure 1.1). At this projected pH, the concentration of CO_3^{2-} will have decreased by 50%. As the CO_3^{2-} concentration decreases, pH will decrease faster upon further anthropogenic CO_2 uptake due to a weakened buffer capacity of the seawater ($\beta = 2.303$ ($[HCO_3^-] + 4[CO_3^{2-}] + [B(OH)_4^-] + [H^+] + [OH^-]$), for a system opened to the atmosphere), causing a dangerous run-away effect (Orr et al., 2005).

1.13 - Alkalinity and the Neutralizing Capacity of the Ocean

Total Alkalinity (TA) is defined as the ability of an aqueous solution to neutralize a strong acid or, in other words, is equal to the sum concentration of all organic and inorganic bases (anions) in a solution that are titratable with a strong acid to an equivalence point corresponding to the conversion of HCO_3^- to H_2CO_3 (Stumm and Morgan, 1996; Gattuso and Hansson, 2011; see Equation 10).

$$TA = [HCO_3^-] + 2[CO_3^{2-}] + [NH_3] + [HS^-] + 2[S^{2-}] + [H_3SiO_4^-] + 2[H_2SiO_4^{2-}] + [B(OH)_4^-] + [Org^-] + [HPO_4^{2-}] + 2[PO_4^{3-}] - [H_3PO_4] + [OH^-] - [H^+] \quad \textbf{(10)}$$

In the open ocean, carbonate alkalinity (Ac) makes up most of its total alkalinity, as the concentration of other bases, apart from the borate ion ($B(OH)_4^-$), are negligible (see Equation 11).

$$[Ac] = [HCO_3^-] + 2[CO_3^{2-}] + [OH^-] - [H^+] = TA - [B(OH)_4^-] \quad \textbf{(11)}$$

The absorption of CO_2 does not affect the alkalinity of seawater unless $CaCO_3$ is precipitated or dissolved (see Equations 1, 3 and 4), it can only affect the pH and, therefore, the speciation of DIC, as seen in Figure 1.1.

1.14 - CO_2 Transport to the Deep Ocean

Carbon delivery from the surface to the deep ocean occurs through two major pathways, or "pumps"; the biological pump (particulate carbon export) and the solubility pump (dissolved carbon export) (see Figure 1.2).

The biological pump refers the production and transport of particulate organic carbon from the ocean's surface to the deep ocean and the seafloor. It can be divided into three major steps; primary production of organic matter (OM; see Equation 12) and carbonate minerals by photosynthetic and higher organisms in the surface ocean, transport of these particles (OM and carbonates) through the water column and, finally, the preservation/decomposition of particles as they settle through the water column and once they reach the seafloor (De La Rocha, 2006).

$$CO_2 + H_2O + light \rightarrow CH_2O + O_2 \quad \textbf{(12)}$$

Part of the organic carbon is remineralized (converted back into CO_2) by microbial oxidation within the water column, the rate of which is controlled by temperature, depth (time of exposure) and the reactivity of the organic matter (Mucci et al., 2000; De La Rocha., 2006; Mouret et al., 2010). The amount of inorganic carbon delivered to the sea floor, in the form of carbonate skeletons/tests, is a function of the surface productivity and the saturation state ($\Omega=[Ca^{2+}][CO_3^{2}]/K^*_{sp}$, where [i] are concentrations and K^*_{sp} is the stoichiometric solubility of calcite or aragonite, the most common $CaCO_3$ polymorphs in marine environments) of the overlying water (Mucci et al., 2000). The final step in the biological pump scenario is the decomposition/preservation of the carbon reaching the seafloor. Organic matter will be subjected

to catabolism through a sequence of microbially-mediated oxidation reactions while the fate of carbonate minerals depends on the saturation state of the overlying waters and sediment pore waters (Froelich et al., 1979; Mucci et al., 2000). These reactions will be discussed in detail later in this thesis.

The solubility pump is a mechanism that describes the transport and cycling of dissolved inorganic carbon throughout the water column. Its mode of operation is dependent on two major factors: the solubility of CO_2 in seawater and the thermohaline circulation within the ocean (Raven and Falkowski, 1999). Given that CO_2 is more soluble in the colder waters of polar regions (North Atlantic, Antarctica/Weddell Sea) where deep, cold marine waters are formed, these areas act as sinks or "doorways" for CO_2 to the deep ocean (Sigman and Boyle, 2000). DIC is then distributed throughout the open ocean through the global, thermohaline circulation.

1.15 - Coastal Systems, Carbon Cycling, Hypoxia and accompanying Acidification

High-latitude coastal regions are most vulnerable to ocean acidification and will be the first to show its most profound impacts (Orr et al., 2005). This is because coastal ocean environments are transition zones or "bridges" between the terrestrial and marine realms (Gattuso et al., 1998; Bauer et al., 2013). In these coastal areas, primary productivity is high and sustained by the delivery of nutrients from the continents or by wind-driven upwelling of CO_2 and nutrient-rich marine waters. The availability of nutrients in the coastal ocean has made it the most productive marine environment in the world, accounting for ~30% of all marine primary productivity despite comprising ~10% of the global ocean's surface area (Gattuso et al., 1998, Gattuso and Hansson, 2011). Estuarine systems are typically supersaturated in CO_2 with respect to the atmosphere and are commonly regarded as a net source of CO_2 to the atmosphere (Gattuso et al., 1998; Bauer et al., 2013). Estuaries are commonly divided into two distinct categories: river-dominated and marine-dominated estuaries. River-dominated estuaries are typically partially mixed, turbid and CO_2 sources to the atmosphere due to microbial respiration and low primary productivity. Marine-dominated estuaries are deeper, stratified, and act as a net sink of atmospheric CO_2 due to biological drawdown (Jiang et al., 2008; Joesof et al., 2015; Dinauer and Mucci, 2017, 2018). The magnitude of CO_2 degassing in individual estuaries is highly variable due to several controlling

factors such as geomorphology (depth and cross-section), hydrology (discharge and flow) and nutrient inputs (Bauer et al., 2013).

Eutrophication results from an increase flux of organic matter (OM) or nutrients, that promote the generation of OM through photosynthesis, to a body of water (Berner and Berner, 1996; Gehlen et al., 2011; Sunda and Cai, 2012). This process may lead to oxygen depletion upon the microbial respiration of the OM and the accompanying accumulation of metabolic CO_2, as in the Gulf of Mexico (Rabalais et al., 2001, 2002) and the Lower St. Lawrence Estuary and Gulf (Mucci et al., 2011). The oxic respiration of OM is represented by the "RKR Equation", as described in Equation 13, using Redfield stoichiometry to represent the chemical composition of algal OM (Redfield et al., 1963). Hedges et al., (2002) proposes a slightly different stoichiometry to this equation, however, for the purpose of this thesis we will use the "RKR" stoichiometry.

$$(CH_2O)_{106}(NH_3)_{16}(H_3PO_4) + 138O_2 \rightleftharpoons 106CO_2 + 16HNO_3 + H_3PO_4 + 122H_2O + trace\ elements \quad \textbf{(13)}$$

Variations in pH depend on which direction the reaction is driven and can greatly intensify the effects of ocean acidification caused from interactions with the atmosphere (Cai et al., 2011; Gattuso and Hansson, 2011; Melzner et al., 2013). The ocean surface waters are in direct contact with the atmosphere, allowing exchange of O_2 and CO_2 across the air-sea interface to counterbalance the above reaction. In a stratified body of water, where mixing is limited by the presence of a strong pycnocline, such as in the open ocean, the Gulf of Mexico (Rabalais et al., 2001, 2002) or the St. Lawrence Estuary (Mucci et al., 2011), oxygen may become depleted and metabolic CO_2 can accumulate in bottom waters. This is reflected by the presence of an oxygen and pH minimum near the permanent thermocline in the open ocean (Poole and Tomczak, 1999) and to the development of hypoxic conditions and the concomitant acidification of bottom waters in the Gulf of Mexico and the St. Lawrence Estuary (Rabalais et al., 2001, 2002; Gilbert et al., 2005; Cai et al., 2011; Mucci et al., 2011).

A water mass is considered hypoxic when the dissolved O_2 concentration falls below 30% saturation and is severely hypoxic when below 20% saturation or 62.5 μmol/L (Rabalais et al.,

1999). This occurs when the rate of organic matter respiration outpaces the replenishment or influx of dissolved O_2 to the water mass. Oxygen depletion in coastal zones occurs at a much faster rate than in the open ocean, largely due to eutrophication and the accompanying rise in primary productivity and organic matter export. The number of documented oxygen-depleted zones in the coastal ocean has multiplied over the past century (Diaz and Rosenberg, 2008; Gilbert et al., 2010). The development of coastal hypoxic environments and the associated acidification has a profound effect on benthic ecosystems, such as making it more difficult or impossible for biocalcification to occur (Kleypas et al., 2006), and reaching lethal DO thresholds where animals can simply no longer survive (i.e. Atlantic Cod in the Lower St. Lawrence Estuary; Plante et al., 1998). This can ultimately limit areas in which these animals can live, changing the overall dynamic of the ecosystem and food web (Diaz and Rosenberg, 2008). In some cases, such as along the Eastern Pacific Shelf, pteropods, the primary food source for juvenile Pacific salmon, will see their calcification and survival increasingly affected by acidification, thus potentially lowering food availability and, therefore, salmon recruitment (Aydin et al., 2005; Comeau et al., 2009).

1.2 - Carbonate Chemistry and Sediments

1.21 - Carbonate Chemistry in Seawater

Carbonate-rich sediments are the ultimate, short-term sink of anthropogenic CO_2. As ocean acidification disrupts the $CaCO_3$ cycle of the ocean, hindering the ability for biogenic organisms to precipitate calcium carbonate skeletons/tests, it also leads to calcium carbonate dissolution if the surrounding waters become undersaturated (i.e., corrosive) with respect to these minerals (Feely et al., 2004; Morse et al., 2007). The chemical reaction that describes the solubility of calcium carbonate minerals in seawater is given by Equation 14.

$$CaCO_3(s) \leftrightarrow Ca^{2+} + CO_3^{2-} \quad \textbf{(14)}$$

The equilibrium constant for this reaction corresponds to the stoichiometric (K^*_{sp}) or thermodynamic (K^o_{sp}) solubility products (see Equations 15 and 16). The thermodynamic solubility product is a function of the temperature (T) and pressure (P) while the stoichiometric

solubility constant also varies with salinity (S). The K^*_{sp} of aragonite and calcite in seawater of various salinities and temperatures was determined by Mucci (1983). The effect of pressure on K^*_{sp} can be calculated from the partial molal volume and compressibility of the reactions, the values of which can be found in Millero (1995). Total ion concentrations are denoted by [i], total ion activities by (i) and total ion activity coefficients by $\gamma_{(i)}$.

$$K^*_{sp} = [Ca^{2+}][CO_3^{2-}] \quad \textbf{(15)}$$

$$K^{o}_{sp} = (Ca^{2+})(CO_3^{2-}) = K^*_{sp}\,\gamma_{Ca^{2+}}\gamma_{CO_3^{2-}} \quad \textbf{(16)}$$

The two most common polymorphs of calcium carbonate that are precipitated by organisms and abiotically in the modern oceans are calcite and aragonite. During precipitation from seawater, calcite will incorporate various amounts of magnesium, as the latter substitutes for calcium in the crystal lattice. The products of these precipitations are called magnesium or magnesian calcites. The solubility of magnesian calcites in seawater at specific T, P and S values depends on the mole fraction of $MgCO_3$ incorporated into the crystal (Busenberg and Plummer, 1989). At lower mole fractions (%$MgCO_3$ <4%), the solubility of calcite is at its lowest, making this the most stable calcium carbonate polymorph. At higher mole fractions (%$MgCO_3$ > ~5%), the solubility of calcite rapidly increases with $MgCO_3$ content, exceeding that of aragonite beyond ~11% $MgCO_3$, making them the least stable common $CaCO_3$ polymorphs in seawater (Morse et al., 2007; Dickson, 2010; see Figure 1.3). At 25°C, aragonite is approximately 50% more soluble than calcite (Mucci, 1983). Therefore, high-magnesian calcites are expected to be the "first responders" to ocean acidification in shallow-water environments where they commonly accumulate (Morse et al., 2006).

The saturation state of seawater with respect calcite or aragonite is defined by:

$$\Omega_x = [Ca^{2+}][CO_3^{2-}]/K^*_{sp(x)} \quad \textbf{(17)}$$

Ω_x is determined by the ratio of the ion concentration product ($[Ca^{2+}][CO_3^{2-}]$) in solution to the stoichiometric solubility product (K^*_{sp}) of the mineral of interest. When the ion concentration product is equal to K^*_{sp}, Ω_x is equal to 1 and the solution is saturated or at equilibrium with respect to calcite or aragonite (Morse et al., 2006; Andersson et al., 2007). If Ω_x is greater than 1, the

solution is supersaturated and precipitation of the stated carbonate mineral should outpace its dissolution. Conversely, if Ω_x is less than 1, the solution is undersaturated with respect to the stated mineral and dissolution should occur if that mineral is present (Morse and Mackenzie, 1990; Morse et al., 2006; Andersson et al., 2007).

Ocean acidification shifts the balance of equations 1, 3 and 4 to favour HCO_3^- and $H_2CO_3^*$, lowering the CO_3^{2-} concentration and saturation state of the seawater with respect to carbonate minerals. Once CO_3^{2-} has become sufficiently depleted, seawater will become undersaturated or corrosive with respect to $CaCO_3$, and its dissolution should occur until saturation is re-established. Hence, ocean acidification will lower the accumulation and preservation of carbonate minerals in sediments.

1.22 - Drivers and Inhibitors of Dissolution

Whereas salinity, pressure and temperature affect the solubility product (K^*_{sp}) of carbonate minerals in seawater, other substances and ions present in the water column/sediments can alter the rate of the reaction, regardless of the saturation state (Terjesen et al., 1961).

1.221 - Magnesium

The incorporation of magnesium into carbonate minerals increases their stoichiometric and thermodynamic solubilities and therefore, decreases their stability (Andersson et al., 2008; Dickson, 2010). The current Mg:Ca ratio in seawater is ~5:1, meaning that many marine organisms incorporate some $MgCO_3$, ranging from ~4% (the most stable) to as high as 30%, into their skeletons/shells (Mackenzie et al., 1983). Davis et al. (2000) determined, through the use of Atomic Force Microscopy (AFM), that the sorption of Mg^{2+} to the crystal surface from the growth solution caused step "pinning" or "blocking", slowing the advancement of crystal steps and therefore inhibiting the precipitation of calcite. This Mg^{2+} is eventually incorporated into the crystal lattice, thus, increasing its solubility (Davis et al., 2000).

1.222 - Phosphate

Soluble reactive phosphate (SRP) is present in trace amounts (0.05-3.0 µmol/L) in seawater and is a very strong inhibitor of calcite dissolution and precipitation (Berner and Morse, 1974; Reddy, 1977). At surface seawater conditions of pH_{Total} = 8.1, S_P = 35 and T = 25°C, orthophosphate or dissolved inorganic phosphate is present in three forms: HPO_4^{2-} (79.2%), PO_4^{3-} (20.4%) and $H_2PO_4^-$ (0.4%), making HPO_4^{2-} the dominant species (Millero, 2013). The influence of SRP on calcite precipitation and dissolution rates has been attributed to its adsorption at high-energy sites on the calcite surface (Millero et al., 2001). This inhibits both growth and dissolution by adsorbing to the edge of steps on the crystal surface and pinning the advancement or retreat of steps (Burton and Walter, 1990; Dove and Hochella, 1993; Xu and Higgins, 2011). Surface waters are typically depleted in SRP, containing <1 µmol/L due to biological uptake, whereas deep marine waters typically contain ~3 µmol/L as organic phosphorus exported with particulate organic matter is remineralized at depth. Sediment pore water SRP concentrations can be tenfold higher due to the accumulation organic matter metabolites (Turekian, 1968; Broecker, 1974). Hence, the presence of high SRP concentrations can contribute to the preservation of carbonate minerals in marine sediments.

1.223 - Dissolved Organic Carbon (DOC)

Dissolved Organic Carbon (DOC) is another inhibitor of calcium carbonate mineral precipitation and dissolution, as its adsorbs to the crystal surface, shielding the mineral from the solution and slowing reaction rates (Chave and Suess, 1970; Morse 1974; Berner et al., 1978; Veetil et al., 2018). Due to the low DOC concentrations in the deep ocean (<1mg/L), Morse (1974) suggested that DOC does not significantly inhibit calcite dissolution/precipitation in the water column, but may do so at the elevated DOC concentrations encountered in most sediment pore waters.

1.23 - Calcium Carbonate Sediments

$CaCO_3$-rich sediments (>30 weight %) cover approximately 30% of the seafloor, making them a ready agent to neutralize anthropogenic CO_2 that is injected into the deep ocean (Archer et al., 1998; see Equation 18).

$$CaCO_3 + CO_{2\,(aq)} + 2H_2O \rightleftharpoons 2HCO_3^- + Ca^{2+} \quad \textbf{(18)}$$

The classic phrase coined by Noel James, "Carbonate sediments are born, not made", powerfully summarizes the nature and genesis of carbonate sediments in the ocean. This holds true as the clear majority (>90%) of modern carbonates are biogenic (exoskeletons and hard parts from marine organisms) and are formed in marine environments known as Carbonate Factories (Tucker and Wright, 1990; James and Jones, 2015).

1.231 - Shallow Carbonate Sediments

The surface ocean is supersaturated with respect to calcium carbonate minerals, allowing them to precipitate in many marine environments. Shallow-water carbonate sediments are characteristic of tropical and sub-tropical environments, but in some cases, may form in more temperate waters or accumulate as detrital materials (Morse and Mackenzie, 1990; Andersson et al., 2003; Mackenzie and Andersson, 2013). Shallow-water carbonate sediments are usually precipitated in carbonate ramp or platform environments (James and Coquette, 1983). Carbonate platforms grow as organisms, such as corals and algae, build reefs and frameworks and broken fragments of skeletal material accumulate at the seafloor. In high energy environments, like the off-shore Bahama Banks, ooids dominate the carbonate sedimentary regime, forming spherical, layered grains (Morse and Mackenzie, 1990). Carbonate sediments precipitated in shallow-water environments are largely composed of aragonite and magnesian calcites (up to 30 mol% Mg) (Morse and Mackenzie, 1990).

1.232 - Deep Carbonate Sediments

Calcium carbonate accumulating in deep-sea sediments of the open ocean is largely composed of low-magnesium calcite tests precipitated in the surface ocean by organisms such as cocolithophores and foraminifera (Morse and Mackenzie, 1990). Aragonite is precipitated largely by pteropods in the open ocean but, due to its elevated solubility, it is rarely preserved in the deep ocean (Morse and Mackenzie, 1990). The surface ocean is supersaturated with respect to calcite and aragonite, where in contrast, the deep ocean is not. This is in great part due to both calcium carbonate polymorphs displaying retrograde solubility; increasing solubility with decreasing temperature and increasing pressure, or in this case, increasing depth in the water column (Millero, 2013). This increase in solubility with depth is complimented by the production of metabolic CO_2 in the water column, due to microbial respiration of settling organic matter, and the resulting decrease in pH and saturation state of seawater with respect to both calcite and aragonite in the oceanic water column (Morse and Mackenzie, 1990; Millero, 2013). The progressive decrease in saturation state with depth in the ocean leads to the establishment of distinct "sediment marker horizons" and the concept of "Carbonate Compensation" as settling $CaCO_3$ particles are preferentially dissolved or preserved in the sediment record (Boudreau et al., 2010). The four major horizons within the deep ocean include the saturation level (aragonite and calcite), the lysocline, the compensation depth (aragonite and calcite) and the snow line (Zeebe and Westbroek, 2003; Millero, 2013). The first and shallowest horizon is the Aragonite Saturation Depth (ASD, $\Omega_A = 1$; ~2500m in Atlantic and <300m in the North Pacific). Coincidently, it typically corresponds to the Aragonite Compensation Depth (ACD), the depth below which little or no aragonite accumulates in sediments. Next is the Calcite Saturation Depth (CSD, $\Omega_C = 1$; ~4000m in Atlantic and <500m in the North Pacific) or R0 level (Broecker and Peng, 1982; Morse and Mackenzie, 1990; Feely et al., 2004). As calcite particles settle beyond this depth, they are subjected to dissolution in the water column. The lysocline follows the CSD and marks the depth where the dissolution rate of calcite increases drastically, decreasing preservation in the sediment by up to 90% (Millero, 2013). The Calcite Compensation Depth (CCD) is defined as the depth where the rate of calcite supply from above is equal to the rate of dissolution. Below this level there is no net accumulation of $CaCO_3$ in the sediments and these typically contain <10% $CaCO_3$ by weight (Broecker and Peng, 1982; Morse and Mackenzie, 1990; Millero, 2013). The final horizon is called the "marine snow

line", beyond this depth sediments are devoid of $CaCO_3$ (Zeebe and Westbrook, 2003; Boudreau et al., 2010).

1.24 - Future changes in Carbonate Chemistry

In all future scenarios for which the atmospheric pCO_2 increases from present day levels, ocean acidification will intensify, as implied by the series of thermodynamic equilibria described in Equations 1-4. These processes, however, do not include other stressors of marine ecosystems such as eutrophication and warming. These can greatly amplify the acidification of coastal environments, such as the St. Lawrence Estuary and Gulf, by increasing the flux of organic material to the system and accelerating its degradation, increasing the rate of metabolic CO_2 accumulation (Gilbert et al., 2005; Doney et al., 2007; Diaz and Rosenberg, 2008; Cai et al., 2011; Mucci et al., 2011). On short time scales (<100 years), the dissolution of carbonate sediments will buffer against the acidification, acting as a sink for CO_2 (Orr, 2011; Mackenzie and Andersson, 2013; see Equation 18).

Several time-series have been constructed based on continued monitoring of seawater pH and pCO_2 at research stations across the world; Hawaii Ocean Time-series (HOT), Bermuda Atlantic Time-series Station (BATS), and the European Station for Time-series Observations in the Ocean (ESTOC). These measurements all show a steady trend within the H_2O-CO_2-$CaCO_3$ system in response to the increase of atmospheric pCO_2, providing the basis for modelling of the evolution of the seawater chemistry on short timescales (centuries) (Bates, 2007; Dore et al., 2008; Mackenzie and Andersson, 2013; see Figure 1.4). This trend is amplified in polar oceans, where $[H_2CO_3^*]$ is inherently higher and $[CO_3^{2-}]$ lower, making them more sensitive to the effects of ocean acidification. Within the next few decades, as the atmospheric pCO_2 keeps increasing, the $[CO_3^{2-}]$ in the surface waters of the polar oceans is expected to drop below the aragonite saturation (Orr, 2011). As $[CO_3^{2-}]$ continues to decrease, a second critical concentration level will be reached where the surface waters will become undersaturated with respect to calcite, making all $CaCO_3$ polymorphs unstable. This scenario could be realized in the polar surface ocean by the end of this century (Orr, 2011; Mackenzie and Andersson, 2013). These conditions will be detrimental to organisms that precipitate carbonate tests, such as pteropods (aragonite), coccolithophores (low

Mg-calcite) and foraminifera (low Mg-calcite), which lie at the base of food chain, as well as other organisms whose physiological functions will be affected by the lower pH of these waters (Fabry et al., 2008; Kroeker et al., 2013).

1.3 - Biogeochemical Processes in Marine Sediments

1.31 - Microbial Respiration and Diagenetic Processes

The preservation of $CaCO_3$ minerals in marine sediments can be influenced by diagenetic processes (Jahnke et al., 1994; Mucci et al., 2000). The most important of these processes is the microbial degradation of organic matter, which is driven by the quantity and reactivity of the OM reaching the seafloor (and temperature). In marine sediments, the sequence of oxidants (or electron-acceptors) used for the microbial degradation of organic matter is dictated by their free energy yield (Claypool and Kaplan, 1974; Froelich et al., 1979). Bacteria first utilize the oxidant that yields the highest free energy until it is depleted, then the next most "energetic" oxidant is used (Froelich et al., 1979). These reactions will proceed until one of two scenarios occurs: (1) all available oxidants are depleted or (2) all reactive organic matter is oxidized (Froelich et al., 1979). Bioturbation affects the mobility of both oxidants (O_2, NO_3^-, Fe(III)/Mn(III) and SO_4^{2-}) and $CaCO_3$ dissolution inhibitors (Mg^{2+}, SRP and DOC) by creating "pathways" for solute exchange across the sediment-water interface (Boudreau et al., 1987; Anschutz et al., 2000; Katsev et al., 2006; Higgins et al., 2009). Calcite dissolution is likely to ensue during aerobic respiration of organic matter as the accumulation of metabolic CO_2 decreases the saturation state of the sediment pore waters and may lead to an undersaturation (Walter and Burton, 1990; Mucci et al., 2000). On the other hand, microbial degradation of organic matter in marine sediments also generates soluble reactive phosphate (SRP) and dissolved organic matter (DOC), both of which can impede the dissolution of $CaCO_3$.

1.32 - Oxic Degradation of Organic Matter

1.321 - Aerobic Respiration

The first and most efficient oxidant used during microbial catabolism of sedimentary organic matter is oxygen (O_2). In an oxygenated water column, the zone of aerobic respiration is located in the uppermost layers of the sediment and typically ranges from a few mm to <10 cm in depth in the coastal ocean (Cai and Reimers, 1995; Cai and Sayles, 1996) to 100s of meters in the abyssal plains of the deep oceans (Burdige, 2006). The thickness of this zone, the oxygen penetration depth in the sediment, depends on several factors (Cai and Sayles, 1996). The first, the sediment oxygen demand, a measure of the bacterial activity, is a function of the amount and reactivity of organic matter delivered to the seafloor as well as temperature. The second, the rate of dissolved oxygen (DO) delivery to the sediment, is a function of the overlying water oxygen concentration, the sediment tortuosity, itself a function of the permeability and porosity of the sediment. The tortuosity affects the diffusion rate of oxygen through the sediment by increasing the diffusional path length (Silverberg et al., 1987; Mouret et al., 2010). Aerobic degradation of organic matter releases metabolic CO_2 to the pore waters, resulting in a drop in pH, and their saturation state with respect to calcite and aragonite (Ω_C and Ω_A) (Froelich et al., 1979; Mucci et al., 2000; Mouret et al., 2010; see Equation 19).

$$(CH_2O)_{106}(NH_3)_{16}H_3PO_4 + 138O_2 \longrightarrow 106HCO_3^- + 16NO_3^- + HPO_4^{2-} + 16H_2O + 124H^+ \quad \textbf{(19)}$$

$$\Delta A_C \downarrow \ , \ pH \downarrow \ , \ \Omega_{C,A} \downarrow$$

1.322 - Denitrification

The reduction of nitrate is the next most energy efficient pathway for the oxidation of organic matter in marine sediments and leads to a drop in pH, carbonate alkalinity (A_C), and saturation state. The abundance of nitrate in marine pore waters (~30 μM), however, is limited relative to oxygen (~350 μM), making for a limited contribution to the overall aerobic oxidation

and a minor impact on the acidification of the pore waters (Froelich et al., 1979; Mucci et al., 2000; see Equation 20).

$$(CH_2O)_{106}(NH_3)_{16}H_3PO_4 + 94.4NO_3^- \longrightarrow \quad \textbf{(20)}$$
$$106HCO_3^- + 55.2N_2 + HPO_4^{2-} + 71.2H_2O + 13.6H^+$$
$$\Delta A_C \uparrow \quad , \quad pH \downarrow \quad , \quad \Omega_{C,A} \downarrow$$

1.33 - Suboxic Degradation of Organic Matter

1.331 - Manganese and Iron Oxide Reduction

Manganese(II) and iron(II) accumulate in sediment pore waters following the microbially-mediated reduction of manganese(III) and iron(III) oxides during suboxic degradation of organic matter (Froelich et al., 1979; Mucci et al., 2000; Thamdrup, 2000; see Equations 21 and 22). The reduction of these metal oxides typically starts below the oxic zone in the sediment profile (Cai and Sayles, 1996). Manganese(III) oxide reduction occurs preferentially over iron(III) oxide due to the higher free energy yield of the oxidation reaction. The extent of both reactions, however, depends on the abundance and reactivity of the various oxides (Froelich et al., 1979). These reactions consume protons from pore waters thus lowering pH, increasing carbonate alkalinity (A_C) and saturation state of pore waters with respect to carbonate minerals, and can, on rare occasions, such as in the Baltic Sea (Sternbeck and Sohlenius, 1997), lead to the precipitation of authigenic carbonates at depth (Mucci et al., 2000). Fe(III) and Mn(III) oxide surfaces have a strong affinity for other ions, particularly oxyanions in solution, leading to a reduced concentration of components such as soluble reactive phosphate, molybdate and arsenate in pore waters (Manning and Goldberg, 1996). Mn(II) accumulating in sediment pore waters can also act as a $CaCO_3$ dissolution inhibitor through adsorption to the mineral surface, thus promoting the preservation of $CaCO_3$ minerals (Arvidson et al., 2003).

$$(CH_2O)_{106}(NH_3)_{16}H_3PO_4 + 236MnO_2 + 364H^+ \longrightarrow \quad \textbf{(21)}$$
$$106HCO_3^- + 236Mn^{2+} + 8N_2 + HPO_4^{2-} + 260H_2O$$
$$\Delta A_C \uparrow \quad , \quad pH \uparrow \quad , \quad \Omega_{C,A} \uparrow$$

$$(CH_2O)_{106}(NH_3)_{16}H_3PO_4 + 424Fe(OH)_3 + 759H^+ \longrightarrow \quad \textbf{(22)}$$
$$106HCO_3^- + 424Fe^{2+} + 16NH_4^+ + HPO_4^{2-} + 1060H_2O$$
$$\Delta A_C \uparrow \ , \ pH \uparrow \ , \ \ \Omega_{C,A} \uparrow$$

1.332 - Sulfate Reduction

Organic matter oxidation by sulfate occurs when the accumulation rate of organic matter surpasses the oxidation potential of oxygen, nitrate and Mn(III)/Fe(III) oxides delivered to the sediment (Froelich et al., 1979; Mucci et al., 2000; see Equation 23). The generation of sulfide can lead to the precipitation of iron monosulfides (FeS) and pyrite (FeS_2). Sulfate itself, however, is a strong inhibitor of $CaCO_3$ dissolution and precipitation, and its presence may result in an increase in the preservation of carbonate minerals (Sjoberg, 1978; Mucci et al., 1989). The reduction of seawater sulfate leads to a minor decrease in pH, but net carbonate alkalinity (A_C) production that will lead to an increase of the saturation state (Ω_C and Ω_A) of the pore waters. Therefore, in the sulfate reduction zone, the precipitation of authigenic carbonate minerals may occur (Froelich et al., 1979; Boudreau and Canfield, 1988; Mucci et al., 2000).

$$(CH_2O)_{106}(NH_3)_{16}H_3PO_4 + 53SO_4^{2-} \longrightarrow \quad \textbf{(23)}$$
$$106HCO_3^- + 53HS^- + 16NH_4^+ + HPO_4^{2-} + 39H^+$$
$$\Delta A_C \uparrow, \ pH \downarrow \ , \ \ \Omega_{C,A} \uparrow$$

1.4 - The St. Lawrence Marine System and Anticosti Island

1.41 - The St. Lawrence Estuary and Gulf

The St. Lawrence Estuary (SLE) is the largest enclosed estuary in the world. It is located in Eastern Canada and links the Great Lakes through the St. Lawrence River to the North Atlantic Ocean (see Figure 1.5). The true estuary starts at the eastern tip of Ile d'Orléans (i.e., first intrusion of seawater), a few kilometers east of Quebec City, and is typically described by three major components; the Upper St. Lawrence Estuary (USLE), from Ile d'Orléans to Tadoussac, the Lower St. Lawrence Estuary (LSLE), from Tadoussac to Pointe-des-Monts, and the Gulf of St. Lawrence

(GSL). The Gulf of St. Lawrence is a partially closed sea, which is connected to the North Atlantic Ocean through the Cabot Strait and the Strait of Belle Isle. The dominant morphological feature of the estuary is the Laurentian Trough, a 1240km long, <500 m deep, submarine canyon, that extends from the continental shelf break to the head of the Lower Estuary at Tadoussac.

The water column within the Laurentian Trough is stratified and defined by three layers during the ice-free season (Dickie and Trites, 1983; Mucci et al., 2011): (1) 25-50 m deep, brackish (S_P ~27-32), surface layer that flows seaward, (2) a saline (S_P ~ 31.5-33), cold (-1 to 2°C), intermediate layer to a depth of ~150 m that forms in the Gulf in the winter and flows landward, (3) a more saline (S_P ~34-35), warm (4 to 7°C), bottom layer below 150 m that originates in the northwestern Atlantic and flows landward at an average rate of ~0.5 cm sec^{-1} (El-Sabh and Silverberg 1990; Bugden, 1991; Gilbert, 2004). The thickness of the surface and intermediate layers vary over the course of the year, combining in the winter due to cooling and separating in the summer (Galbraith, 2006). The composition of the deep waters is the product of mixing, between the Labrador Current (LCW) and the North Atlantic Central Waters (NACW), at the edge of the continental shelf before entering the Gulf of St. Lawrence through the Cabot Strait (Bugden, 1991; Gilbert et al., 2005). The LCW is cooler and oxygen-rich compared to the NACW. In the early 1930's, the LCW accounted for ~72% of the deep-water mixture entering the Gulf of St. Lawrence, but the mixing ratios have changed over time. In 2005, the mixing ratio was estimated at 53% LCW to 47% of the warmer, oxygen-depleted NACW, leading to a progressive decrease in the amount of oxygen supplied to the deep waters entering the GSL (Gilbert et al., 2005). The dissolved oxygen of these deep waters is gradually consumed as they flow landward as a result of the microbial degradation of organic matter (Benoit et al., 2006; Thibodeau et al., 2006; Genovesi et al., 2011). Due to the permanently stratified structure of the water column in the SLE, replenishment of dissolved oxygen in the bottom waters occurs by slow diffusion and turbulent mixing from the surface waters (Bugden, 1991). Over the past century, the combination of changes in the mixing ratio of the source waters at depth and increased microbial respiration rates has led to the depletion of oxygen in the GSL and the development of persistent hypoxia in the LSLE (Gilbert et al., 2005; Genovesi et al., 2011; Lefort et al., 2012; see Figure 1.6). The accumulation of metabolic CO_2 in the bottom waters of the LSLE and GSL has led to their acidification, mimicking conditions predicted for the surface ocean by the end of this century (Mucci et al.,

2011). Hence, the recruitment, growth, metabolism and survival of calcifying invertebrates and other benthic organisms exposed to these waters could be deleteriously affected (Kuhihara, 2008; Gazeau et al., 2010; Talmage et al., 2010; Parker et al. 2012). Biogenic carbonate minerals, however, are almost absent within the Laurentian Trough sediments, except for detrital carbonates being eroded from Anticosti Island and episodic coccolithophore blooms in the vicinity of the Belle Isle Strait (Levasseur et al., 1994; Fuentes-Yaco et al., 1997; Levasseur et al., 1997).

1.42 - Anticosti Island

Anticosti Island is located off the coast of Quebec, Canada in the Gulf of St. Lawrence. It is 222 km long and 56 km wide (James et al., 2015). The island is composed of a well preserved, 900 m thick, package of Upper Ordovician and Lower Silurian sedimentary rocks and is considered to be the best representation of the Ordovician-Silurian Boundary in the world (Orth et al., 1986; Desrochers, 2006; Desrochers et al., 2010; James et al., 2015). The stratigraphy of Anticosti Island describes a south-westward dipping, shallow, carbonate ramp that was originally deposited in a tropical environment in the northern Iapetus Ocean (Long et al., 1987; Long, 1993; Desrochers, 2006; James et al., 2015). The Ordovician and Silurian periods were much different than the modern environment, and are considered to be in a phase known a "Calcite Sea" where the seawater Mg:Ca ratio was ~1:1, in contrast to 5:1 today, and low magnesium calcite (LMC) was the readily precipitated carbonate mineral. Any aragonite or high magnesium calcites (HMC) would presumably have been subsequently recrystallized or dissolved (Stanley and Hardie, 1998; James et al., 2015). Atmospheric pCO_2 levels are estimated to have been as much as 10 times higher than present day values (Berner, 2004).

1.5 - Research Objectives and Rationale

Over the past century, minimum dissolved oxygen concentrations (DO) in the bottom waters of the Lower St. Lawrence Estuary (LSLE) and the Gulf have decreased dramatically from 125 µmol/L in the 1930's, to values as low as 60 µmol/L in the early 1980's, 51.2 µmol/L in 2003 and the lowest value recorded of 49.4 µmol/L in 2017 (Gilbert et al., 2005; Mucci et al., 2011). Oxygen depletion has been attributed primarily to changes in the mixing ratios, on the eastern

Canadian continental margin at the entrance to the Gulf of St. Lawrence, of the two major source-water masses: the Labrador Current Water (LCW) and the North Atlantic Central Water (NACW). These two water masses make up the deep water that enters the Gulf of St. Lawrence and St. Lawrence Estuary through the Cabot Strait (Gilbert et al., 2005). The remaining depletion of oxygen is caused by the microbially-mediated oxidation of organic matter settling from the surface, coupled with a poorly ventilated, heavily stratified water column. This has led to the accumulation of metabolic CO_2 in the bottom waters, their acidification and a decrease in pH (0.3-0.4 pH unit). The latter is commensurate to the variation expected for average oceanic surface waters by the end of this century, making this setting an analogue for ocean acidification and its future impacts (Mucci et al., 2011). The decrease in pH is accompanied by a decrease in the carbonate ion concentration and the saturation state of the waters with respect to both calcite and aragonite (Ω_C and Ω_A). Although the Laurentian Trough sediments are mostly devoid of calcium carbonate fossils, detrital (Ordovician/Silurian) carbonates originating from Anticosti Island accumulate on the neighboring seafloor.

Though aragonite is absent from these sediments, the fate of the detrital calcite has yet to be documented. Therefore, the main objective of this thesis is to determine if and how the development of oxygen-depleted bottom waters of the St. Lawrence Estuary and Gulf, and the concomitant acidification as a result of metabolic CO_2 accumulation, is affecting the preservation of detrital carbonates that have accumulated off the coast of Anticosti Island. This overarching objective has led to the formulation of three primary research questions:

(1) Can evidence of carbonate dissolution be observed in solid-phase and pore water profiles of the neighboring sediments?

(2) Has preservation of carbonate minerals in the Gulf of the St. Lawrence sediment decreased over time?

(3) How does the preservation of calcium carbonate vary spatially within the Gulf of the St. Lawrence?

The results and methodology of this thesis are compiled in the form of an academic manuscript in Chapter 2. The manuscript, titled “The Impact of Oxygen Depletion and the

Concomitant Acidification of Bottom Waters on the Preservation of Detrital Carbonates in the Gulf of St. Lawrence", explores and answers the above questions in detail. The final section of this thesis (Chapter 3) includes a set of general conclusions, a summary of the work and recommendations for future research.

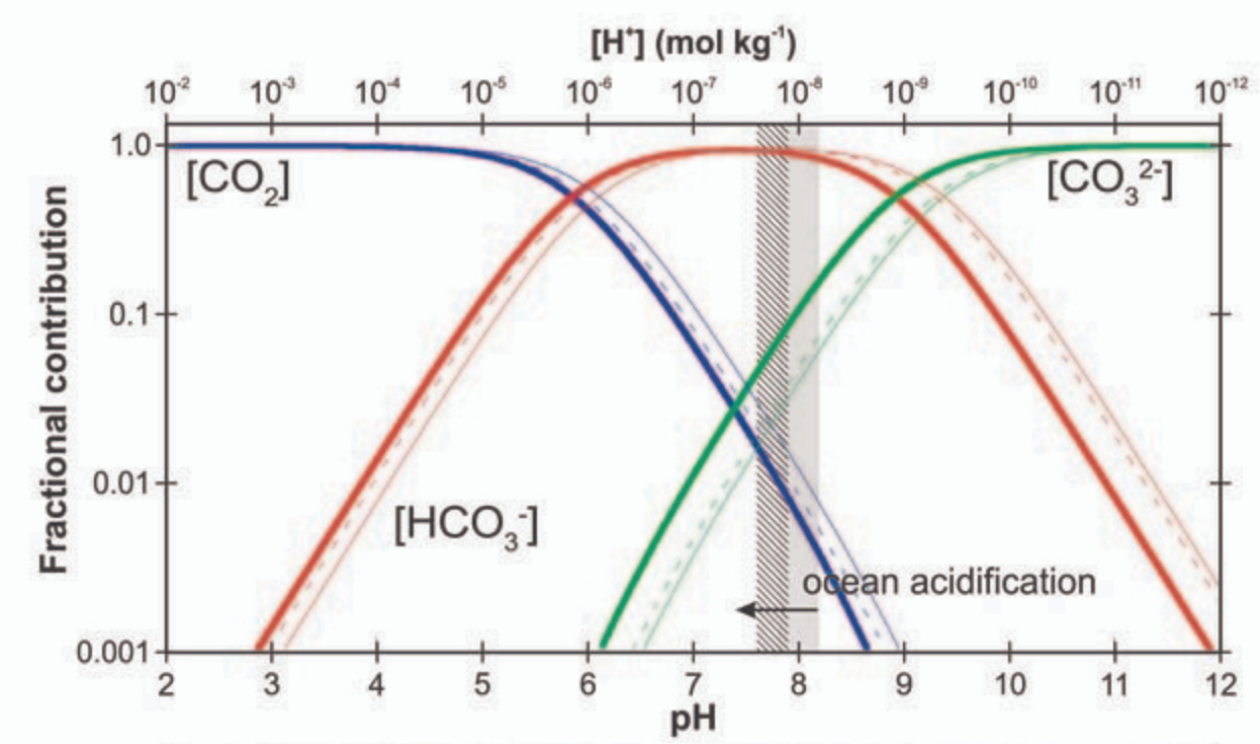

Figure 1.1: Bjerrum/speciation diagram of DIC under varying environmental conditions (Bold lines are for S_P =35, T=25ºC, P = 1 bar, thin lines are for S=35, T=0ºC, P= 1 bar, dashed lines are for S_P=35, T=0ºC and P=300 bar) The shaded region represents the current, annual range of ocean surface pH_T (Average=8.1, total proton concentration scale defined under the constant ionic medium convention). The hashed region represents the projected range for the year 2100 (Barker and Ridgwell, 2012).

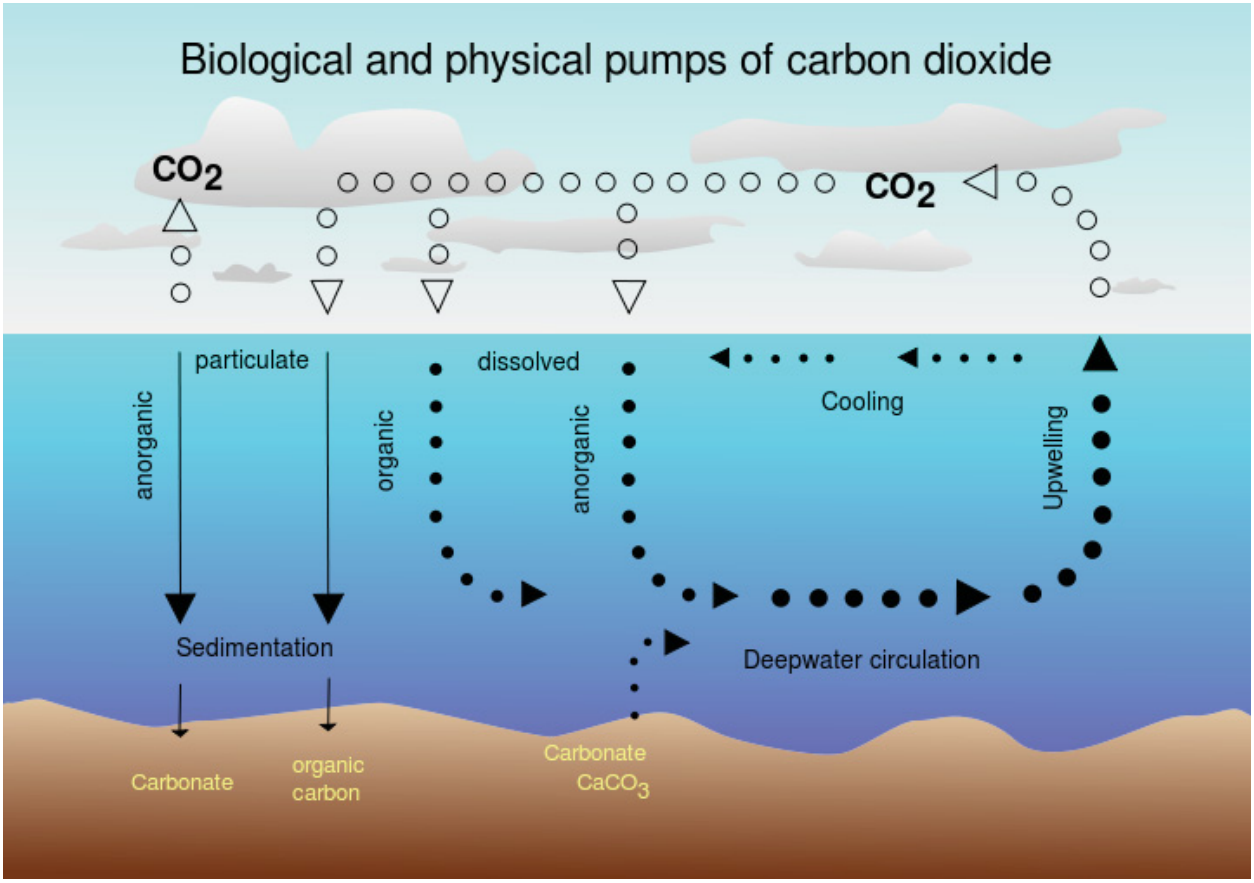

Figure 1.2: Air-sea exchange of carbon dioxide along with the biological and physical pump systems (Hannes Grobe, Alfred Wegener Institute for Polar and Marine Research, taken from https://commons.wikimedia.org/wiki/File:CO2_pump_hg.png).

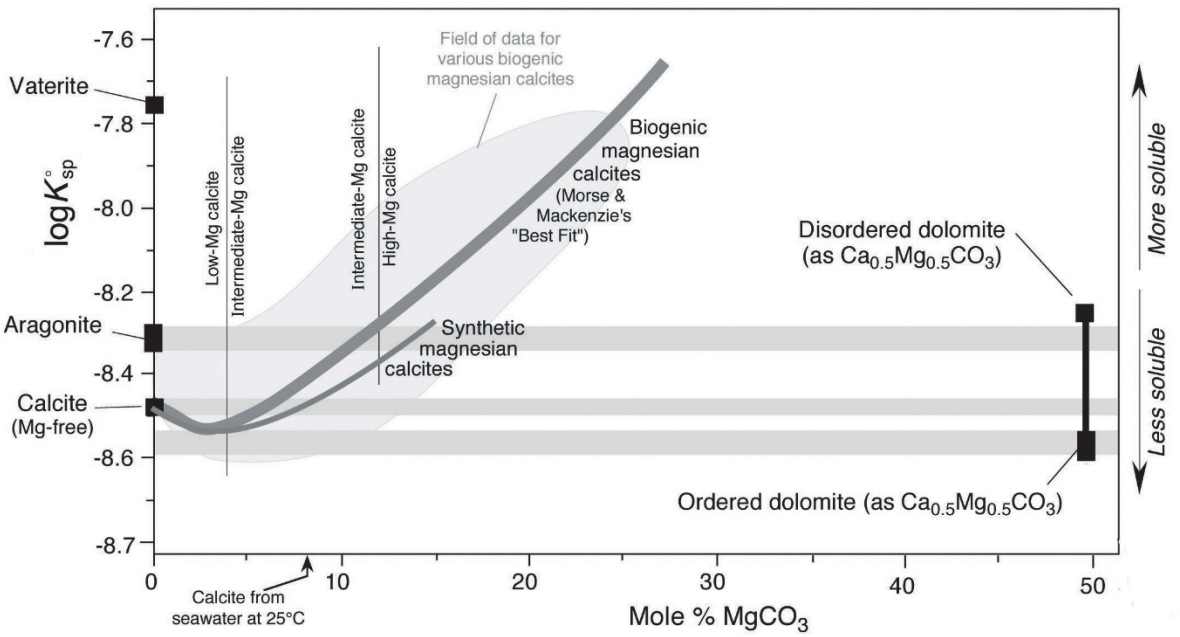

Figure 1.3: The thermodynamic solubility of aragonite, calcite and magnesian calcites at 25°C (Dickson, 2010).

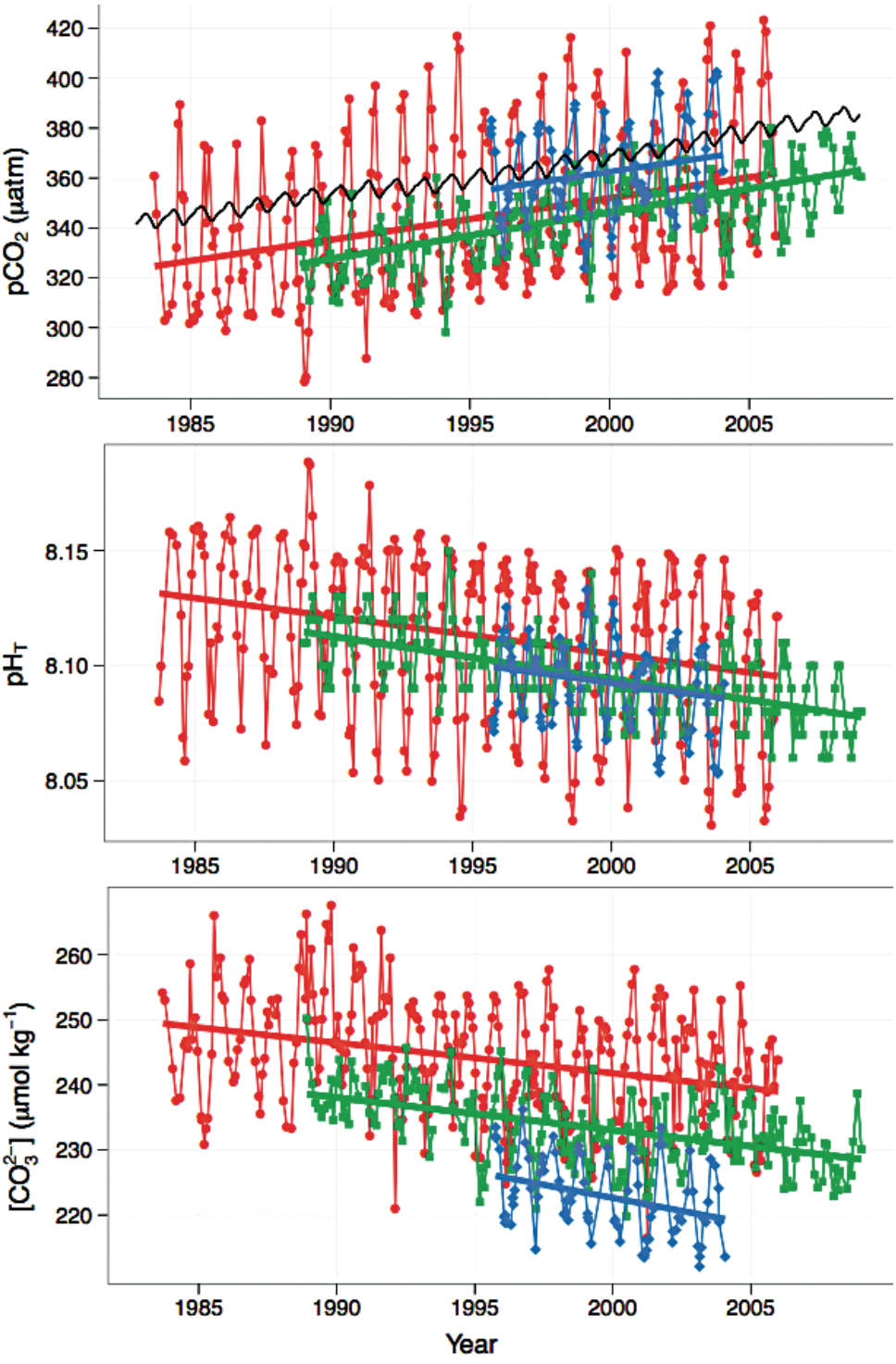

Figure 1.4: Surface ocean pCO_2, pH_T, and $[CO_3^{2-}]$ as recorded at the Bermuda Atlantic Time-Series Station (BATS; red), the Hawaii Ocean Time-series (ALOHA; green), and the European Station for Time-series Observations in the Ocean (ESTOC; blue) over the past few decades. Atmospheric pCO_2 is shown in lockstep with pCO_2 in the ocean by the black line (Mackenzie and Andersson, 2013).

Figure 1.5: Map of the St. Lawrence Marine System, including the Great Lakes, St. Lawrence River, Upper St. Lawrence Estuary (USLE), Lower St. Lawrence Estuary (LSLE) and Gulf of St. Lawrence (GSL) (Overview of the state of the St. Lawrence River, 2014).

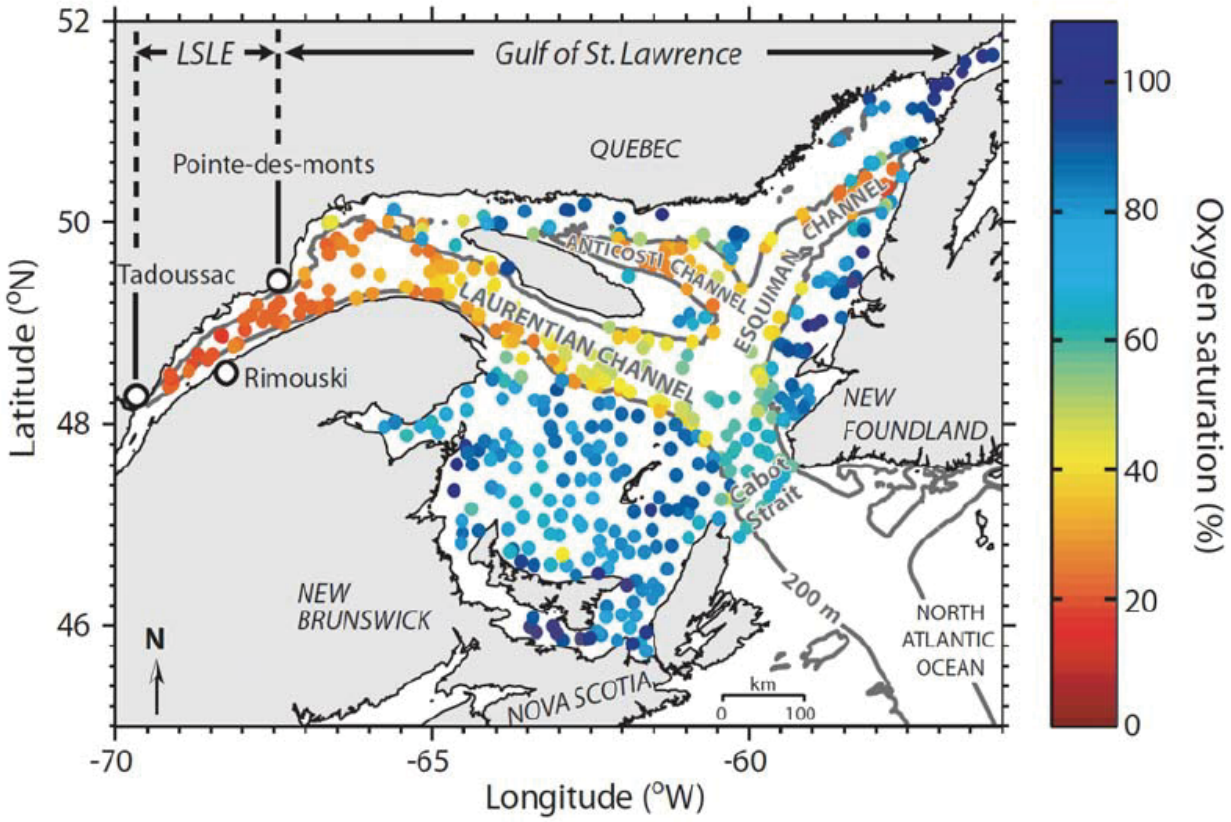

Figure 1.6: Map of the Lower St. Lawrence Estuary (LSLE) and the Gulf of St. Lawrence (GSL), showing the Laurentian Channel and the oxygen saturation of the bottom waters (Gilbert et al., 2007).

1.6 - References

Andersson, A. J., Mackenzie, F. T., & Ver, L. M. (2003). Solution of shallow-water carbonates: An insignificant buffer against rising atmospheric CO_2. Geology, 31(6), 513-516.

Andersson, A. J., Bates, N. R., & Mackenzie, F. T. (2007). Dissolution of carbonate sediments under rising pCO_2 and ocean acidification: observations from Devil's Hole, Bermuda. Aquatic Geochemistry, 13(3), 237-264.

Andersson, A. J., Mackenzie, F. T., & Bates, N. R. (2008). Life on the margin: implications of ocean acidification on Mg-calcite, high latitude and cold-water marine calcifiers. Marine Ecology Progress Series, 373, 265-274.

Anschutz, P., Sundby, B., Lefrancois, L., Luther III, G. W., & Mucci, A. (2000). Interactions between metal oxides and species of nitrogen and iodine in bioturbated marine sediments. Geochimica et Cosmochimica Acta, 64(16), 2751-2763.

Archer, D., Kheshgi, H., & Maier-Reimer, E. (1998). Dynamics of fossil fuel CO_2 neutralization by marine $CaCO_3$. Global Biogeochemical Cycles, 12(2), 259-276.

Arvidson, R. S., Ertan, I. E., Amonette, J. E., & Luttge, A. (2003). Variation in calcite dissolution rates: A fundamental problem? Geochimica et Cosmochimica Acta, 67(9), 1623-1634.

Aydin, K. Y., McFarlane, G. A., King, J. R., Megrey, B. A., & Myers, K. W. (2005). Linking oceanic food webs to coastal production and growth rates of Pacific salmon (*Oncorhynchus* spp.), using models on three scales. Deep Sea Research Part II: Topical Studies in Oceanography, 52(5-6), 757-780.

Barker, S. & Ridgwell, A. (2012) Ocean Acidification. Nature Education Knowledge, 3(10), 21.

Bates, N. R. (2007). Interannual variability of the oceanic CO_2 sink in the subtropical gyre of the North Atlantic Ocean over the last 2 decades. Journal of Geophysical Research, Oceans, 112(C9).

Bauer, J. E., Cai, W. J., Raymond, P. A., Bianchi, T. S., Hopkinson, C. S., & Regnier, P. A. (2013). The changing carbon cycle of the coastal ocean. Nature, 504(7478), 61-70. 10.1038/nature12857.

Benoit P., Gratton Y. & Mucci A. (2006). Modeling of dissolved oxygen levels in the bottom waters of the Lower St. Lawrence Estuary: coupling of benthic and pelagic processes. Marine Chemistry, 102, 13-32.

Berner, R. A., & Morse, J. W. (1974). Dissolution kinetics of calcium carbonate in sea water; IV, Theory of calcite dissolution. American Journal of Science, 274(2), 108-134.

Berner, R. A., Westrich, J. T., Graber, R., Smith, J., & Martens, C. S. (1978). Inhibition of aragonite precipitation from supersaturated seawater; a laboratory and field study. American Journal of Science, 278(6), 816-837.

Berner, R. A. (2004). The Phanerozoic carbon cycle: CO_2 and O_2. Oxford University Press, New York, 147p.

Berner, E., & Berner, R. (1996). Global Environment Water, Air, and Geochemical Cycles Prentice-Hall. Englewood Cliffs, New Jersey, 488p.

Boudreau, B.P. (1987). A steady-state diagenetic model for dissolved carbonate species and pH in the porewaters of oxic and suboxic sediments. Geochimica et Cosmochimica Acta, 51, 1985–1996.

Boudreau, B. P., & Canfield, D. E. (1988). A provisional diagenetic model for pH in anoxic porewaters: Application to the FOAM site. Journal of Marine Research, 46(2), 429-455.

Boudreau, B. P., Middelburg, J. J., & Meysman, F. J. (2010). Carbonate compensation dynamics. Geophysical Research Letters, 37(3).

Burton, E. A., & Walter, L. M. (1990). The role of pH in phosphate inhibition of calcite and aragonite precipitation rates in seawater. Geochimica et Cosmochimica Acta, 54(3), 797-808.

Busenberg, E., & Plummer, L. N. (1989). Thermodynamics of magnesian calcite solid-solutions at 25 C and 1 atm total pressure. Geochimica et Cosmochimica Acta, 53(6), 1189-1208.

Broecker, W. S., & Peng, T. H. (1982). Tracers in the Sea. Lamont-Doherty Geological Observatory, Palisades, New York, 384p.

Bugden, G. L. (1991). Changes in the temperature-salinity characteristics of the deeper waters of the Gulf of St. Lawrence over the past several decades. In: Therriault, J. (Eds.) The Gulf of St. Lawrence: Small Ocean or Big Estuary, (113), 139-147.

Burdige, D.J., 2006. Geochemistry of Marine Sediments. Princeton University Press Princeton, NJ, 624 p.

Cai, W. J., & Reimers, C. E. (1995). Benthic oxygen flux, bottom water oxygen concentration and core top organic carbon content in the deep northeast Pacific Ocean. Deep Sea Research Part I: Oceanographic Research Papers, 42(10), 1681-1699.

Cai, W.J. & Sayles, F.L., (1996). Oxygen penetration depths and fluxes in marine sediments. Marine Chemistry, 52, 123–131.

Cai, W.J., Hu, X., Huang, W.J., Murrell, M.C., Lehrter, J.C., Lohrenz, S.E., Chou, W.C., Zhai, W., Hollibaugh, J.T., Wang, Y. and Zhao, P. (2011). Acidification of subsurface coastal waters enhanced by eutrophication. Nature Geoscience, 4, 766–770.

Caldeira, K., & Wickett, M. E. (2005). Ocean model predictions of chemistry changes from carbon dioxide emissions to the atmosphere and ocean. Journal of Geophysical Research, Oceans, 110(C9), doi:10.1029/2004JC002671.

Chave, K. E., & Suess, E. (1970). Calcium carbonate saturation in seawater: effects of dissolved organic matter. Limnology and Oceanography, 15(4), 633-637.

Claypool G.E., & Kaplan I.R. (1974). The Origin and Distribution of Methane in Marine Sediments. In: Kaplan I.R. (Eds.) Natural Gases in Marine Sediments. Marine Science, 3, 99-139. Springer, Boston, MA.

Comeau, S., Gorsky, G., Jeffree, R., Teyssié, J. L., & Gattuso, J. P. (2009). Impact of ocean acidification on a key Arctic pelagic mollusc (*Limacina helicina*). Biogeosciences, 6(9), 1877-1882.

Davis, K. J., Dove, P. M., & De Yoreo, J. J. (2000). The role of Mg^{2+} as an impurity in calcite growth. Science, 290(5494), 1134-1137.

De La Rocha, C. L. (2006). Description of the Biological Pump. In: Elderfield, H. (Ed), The Oceans and Marine Geochemistry, 6, 83-107. Elsevier Scientific Publication, Amsterdam, The Netherlands.

Diaz, R. J., & Rosenberg, R. (2008). Spreading dead zones and consequences for marine ecosystems. Science, 321(5891), 926-929.

Desrochers, A. (2006). Rocky shoreline deposits in the lower Silurian (upper Llandovery, Telychian) Chicotte formation, Anticosti island, Quebec. Canadian Journal of Earth Sciences, 43(8), 1205-1214.

Desrochers, A., Farley, C., Achab, A., Asselin, E., & Riva, J. F. (2010). A far-field record of the end Ordovician glaciation: the Ellis Bay Formation, Anticosti Island, Eastern Canada. Palaeogeography, Palaeoclimatology, Palaeoecology, 296(3), 248-263.

Dickie, L. & R.W. Trites. (1983). The Gulf Of St. Lawrence. In: L. Dickie & R.W. Trites (Eds.), Estuaries and Semi-Enclosed Seas, 403-425, Elsevier Scientific Publication, Amsterdam, The Netherlands.

Dickson, A.G. (1984). pH scales and proton-transfer reactions in saline media such as sea water. Geochimica et Cosmochimica Acta, 48(11), 2299-2308.

Dickson, A.G. (2010). The carbon dioxide system in seawater: equilibrium chemistry and measurements. In: Riebesell U., Fabry V.J., Hansson L, Gattuso J.P., (Eds.), Guide to best practices for ocean acidification research and data reporting, 17-40. Publications Office of the European Union, Luxembourg.

Dinauer, A., & Mucci, A. (2017). Spatial variability in surface-water pCO_2 and gas exchange in the world's largest semi-enclosed estuarine system: St. Lawrence Estuary (Canada). Biogeosciences, 14(13), 3221.

Dinauer, A., & Mucci, A. (2018). Distinguishing between physical and biological controls on the spatial variability of pCO_2: A novel approach using OMP water mass analysis (St. Lawrence, Canada). Marine Chemistry, doi:10.1016/j.marchem.2018.03.007

Doney, S. C., Mahowald, N., Lima, I., Feely, R. A., Mackenzie, F. T., Lamarque, J. F., & Rasch, P. J. (2007). Impact of anthropogenic atmospheric nitrogen and sulfur deposition on ocean acidification and the inorganic carbon system. Proceedings of the National Academy of Sciences, 104(37), 14580-14585.

Doney, S. C., Fabry, V. J., Feely, R. A., & Kleypas, J. A. (2009). Ocean acidification: the other CO_2 problem, Annual Review in Marine Sciences, 1: 169-192. doi:10.1146/annurev.marine.010908.163834

Dore, J. E., Letelier, R. M., Church, M. J., Lukas, R., & Karl, D. M. (2008). Summer phytoplankton blooms in the oligotrophic North Pacific Subtropical Gyre: Historical perspective and recent observations. Progress in Oceanography, 76(1), 2-38.

El-Sahb, M.I., & Silverberg, N. (1990). The St. Lawrence Estuary: Introduction. In: M.I. El-Sabh & N. Silverberg (Eds.), Oceanography of a Large-scale Estuarine System, 1-9. Springer-Verlag, New York.

Fabry, V.J., Seibel, B.A., Feely, R.A., & Orr, J.C. (2008). Impacts of ocean acidification on marine fauna and ecosystem processes. ICES Journal of Marine Science, 65, 414-432.

Feely, R. A., Sabine, C. L., Lee, K., Berelson, W., Kleypas, J., Fabry, V. J., & Millero, F. J. (2004). Impact of anthropogenic CO_2 on the $CaCO_3$ system in the oceans. Science, 305(5682), 362-366.

Feely, R. A., Doney, S. C., & Cooley, S. R. (2009). Ocean acidification: Present conditions and future changes in a high-CO_2 world. Oceanography, 22(4), 36-47.

Froelich, P., Klinkhammer, G. P., Bender, M. L., Luedtke, N. A., Heath, G. R., Cullen, D., Dauphin, P., Hammond, D., Hartman, B., & Maynard, V. (1979). Early oxidation of organic matter in pelagic sediments of the eastern equatorial Atlantic: suboxic diagenesis. Geochimica et Cosmochimica Acta, 43(7), 1075-1090.

Fuentes-Yaco, C., Vézina, A. F., Larouche, P., Vigneau, C., Gosselin, M., & Levasseur, M. (1997). Phytoplankton pigment in the Gulf of St. Lawrence, Canada, as determined by the Coastal Zone Color Scanner—part I: Spatio-temporal variability. Continental Shelf Research, 17(12), 1421-1439.

Galbraith, P. S. (2006). Winter water masses in the Gulf of St. Lawrence. Journal of Geophysical Research: Oceans, 111(C6).

Gattuso, J. P., Frankignoulle, M., & Wollast, R. (1998). Carbon and carbonate metabolism in coastal aquatic ecosystems. Annual Review of Ecology and Systematics, 29(1), 405-434.

Gattuso, J. P., & Hansson, L. (2011). Ocean acidification: background and history. In: Gattuso, J.P., & Hansson, L. (Eds.), Ocean acidification, 1-20. Oxford University Press, New York.

Gazeau, F., Parker, L.M., Comeau, S., Gattuso, J.-P., O'Connor, W.A., Martin, S., Pörtner, H. O., and Ross, P.M. (2013). Impacts of ocean acidification on marine shelled molluscs. Marine Biology, 160, 2207–2245.

Gehlen, M., Gruber, N., Gangstø, R., Bopp, L., & Oschlies, A. (2011). Biogeochemical consequences of ocean acidification and feedbacks to the earth system. In: Gattuso, J.P., & Hansson, L. (Ed), Ocean acidification, 230-248. Oxford University Press, New York.

Genovesi, L., de Vernal, A., Thibodeau, B., Hillaire-Marcel, C., Mucci, A. & Gilbert, D. (2011). Recent changes in bottom water oxygenation and temperature in the Gulf of St. Lawrence: micropaleontological and geochemical evidence. Limnology and Oceanography 56(4), 1319-1329.

Gilbert, D. (2004). Propagation of temperature signals along the northwest Atlantic continental shelf edge and into the Laurentian Channel. Abstract, ICES CIEM Annual Science Conference September 22–25, Vigo, Spain.

Gilbert, D., Sundby, B., Gobeil, C., Mucci, A., & Tremblay, G. H. (2005). A seventy-two-year record of diminishing deep-water oxygen in the St. Lawrence Estuary: The northwest Atlantic connection. Limnology and Oceanography, 50(5), 1654-1666.

Gilbert, D., Chabot, D., Archambault, P., Rondeau, B., & Hébert, S. (2007). Appauvrissement en oxygène dans les eaux profondes du Saint-Laurent marin: causes possibles et impacts écologiques. Naturaliste Canadien, 131, 67-75.

Gilbert, D., Rabalais, N. N., Diaz, R. J. & Zhang, J. (2010). Evidence for greater oxygen decline rates in the coastal ocean than in the open ocean. Biogeosciences, 7, 2283–2296.

Hedges, J. I., Baldock, J. A., Gélinas, Y., Lee, C., Peterson, M. L., & Wakeham, S. G. (2002). The biochemical and elemental compositions of marine plankton: A NMR perspective. Marine Chemistry, 78(1), 47-63.

Higgins, J. A., Fischer, W. W., & Schrag, D. P. (2009). Oxygenation of the ocean and sediments: consequences for the seafloor carbonate factory. Earth and Planetary Science Letters, 284(1-2), 25-33.

IPCC. (2007). Climate change 2007: the scientific basis. Contribution of Working Group I to the Fourth Assessment Report of the Intergovernmental Panel on Climate Change. Cambridge University Press, New York.

James, N. P., & Choquette, P. W. (1983). Diagenesis 6. Limestones—The sea floor diagenetic environment. Geoscience Canada, 10(4), 162-179.

James, N. P., Desrochers, A., & Kyser, T. K. (2015). Polygenetic (Polyphase) Karsted Hardground Omission Surfaces In: Lower Silurian Neritic Limestones: Anticosti Island, Eastern Canada. Journal of Sedimentary Research, 85(9), 1138-1154.

James, N. P., & Jones, B. (2015). Origin of Carbonate Rocks. John Wiley & Sons, Oxford, 445p.

Jiang, L. Q., Cai, W. J., & Wang, Y. (2008). A comparative study of carbon dioxide degassing in river-and marine-dominated estuaries. Limnology and Oceanography, 53, 2603–2615.

Joesoef, A., Huang, W. J., Gao, Y., & Cai, W. J. (2015). Air–water fluxes and sources of carbon dioxide in the Delaware Estuary: spatial and seasonal variability. Biogeosciences, 12, 6085–6101.

Katsev, S., Sundby, B., & Mucci, A. (2006). Modeling vertical excursions of the redox boundary in sediments: Application to deep basins of the Arctic Ocean. Limnology and Oceanography, 51(4), 1581-1593.

Kleypas, J.A., Feely, R.A., Fabry, V.J. , Langdon, C., Sabine, C.L., and & Robbins, L.L. (2006). Impacts of Ocean Acidification on Coral Reefs and Other Marine Calcifiers: A Guide for Future Research, report of a workshop held 18–20 April 2005, St. Petersburg, FL, sponsored by NSF, NOAA, and the U.S. Geological Survey, 88 p.

Koutitonsky, V. G., & Bugden, G. L. (1991). The physical oceanography of the Gulf of St. Lawrence: a review with emphasis on the synoptic variability of the motion. In: Therriault, J. (Eds.) The Gulf of St. Lawrence: Small Ocean or Big Estuary, 113, 57-90.

Kroeker, K.J., Kordas, R.L., Crim, R., Hendriks, E., Ramajo, L., Singh, G.D., Duarte, C.M., & Gattuso, J.P. (2013). Impacts of ocean acidification on marine organisms: quantifying sensitivities and interaction with warming. Global Change Biology, 19, 1888-1896.

Kurihara, H. (2008). Effects of CO_2-driven ocean acidification on the early developmental stages of invertebrates. Marine Ecology Progress Series, 373, 275-284.

Le Quéré, C., Raupach, M. R., Canadell, J. G., Marland, G., Le Quéré et al, C., Le Quéré et al, C., Raupach, M. R., Canadell, J. G., Marland, G., Bopp, L., Ciais, P., Conway, T. J., Doney, S. C., Feely, R. A., Foster, P., Friedlingstein, P., Gurney, K., Houghton, R. A., House, J. I., Huntingford, C., Levy, P. E., Lomas, M. R., Majkut, J., Metzl, N., Ometto, J. P., Peters, G. P., Prentice, I. C., Randerson, J. T., Running, S. W., Sarmiento, J. L., Schuster, U., Sitch, S., Takahashi, T., Viovy, N., van der Werf, G. R., Woodward, F. I., & et al. (2009). Trends in the sources and sinks of carbon dioxide: Nature Geoscience, 2(12), 831-836.

Lefort, S., Gratton, Y., Mucci, A., Dadou, I., & Gilbert, D. (2012). Hypoxia in the Lower St. Lawrence Estuary: How physics controls spatial patterns. Journal of Geophysical Research: Oceans, 117(C7).

Levasseur, M., Keller, M. D., Bonneau, E., D'amours, D., & Bellows, W. K. (1994). Oceanographic basis of a DMS-related Atlantic cod (*Gadus morhua*) fishery problem: blackberry feed. Canadian Journal of Fisheries and Aquatic Sciences, 51(4), 881-889.

Levasseur, M., Sharma, S., Cantin, G., Michaud, S., Gosselin, M., & Barrie, L. (1997). Biogenic sulfur emissions from the Gulf of Saint Lawrence and assessment of its impact on the Canadian east coast. Journal of Geophysical Research: Atmospheres, 102(D23), 28025-28039.

Long, D. G. F., & Copper, P. (1987). Stratigraphy of the Upper Ordovician upper Vaureal and Ellis Bay formations, eastern Anticosti Island, Quebec. Canadian Journal of Earth Sciences, 24(9), 1807-1820.

Long, D. G. (1993). Oxygen and carbon isotopes and event stratigraphy near the Ordovician—Silurian boundary, Anticosti Island Quebec. Palaeogeography, Palaeoclimatology, Palaeoecology, 104(1-4), 49-59.

Mackenzie, F. T., Bischoff, W. D., Bishop, F. C., Loijens, M., Schoonmaker, J., & Wollast, R. (1983). Magnesian calcites; low-temperature occurrence, solubility and solid-solution behavior. Reviews in Mineralogy and Geochemistry, 11(1), 97-144.

Mackenzie, F. T., & Andersson, A. J. (2013). The marine carbon system and ocean acidification during Phanerozoic time. Geochemical Perspectives, 2(1), 1-3.

Manning, B. A., & Goldberg, S. (1996). Modeling competitive adsorption of arsenate with phosphate and molybdate on oxide minerals. Soil Science Society of America Journal, 60(1), 121-131.

Melzner, F., Thomsen, J., Koeve, W., Oschlies, A., Gutowska, M.A., Bange, H.W., Hansen, H.P., and Körtzinger, A. (2013). Future ocean acidification will be amplified by hypoxia in coastal habitats. Marine Biology, 160, 1875–1888

Miller, A. W., Reynolds, A. C., Sobrino, C., & Riedel, G. F. (2009). Shellfish face uncertain future in high CO_2 world: influence of acidification on oyster larvae calcification and growth in estuaries. PloS ONE, 4(5), e5661.

Millero, F. J. (1995). Thermodynamics of the carbon dioxide system in the oceans. Geochimica et Cosmochimica Acta, 59(4), 661-677.

Millero, F., Huang, F., Zhu, X., Liu, X., & Zhang, J. Z. (2001). Adsorption and desorption of phosphate on calcite and aragonite in seawater. Aquatic Geochemistry, 7(1), 33-56.

Millero, F. J., Pierrot, D., Lee, K., Wanninkhof, R., Feely, R., Sabine, C. L., Key, R. M., & Takahashi, T. (2002). Dissociation constants for carbonic acid determined from field measurements. Deep Sea Research Part I: Oceanographic Research Papers, 49(10), 1705-1723.

Millero, F.J. (2013). Chemical Oceanography. CRC Press, Taylor & Francis Group, Boca Raton, FL, 591 pp.

Morse, J. W. (1974). Dissolution kinetics of calcium carbonate in sea water; V, effects of natural inhibitors and the position of the chemical lysocline. American Journal of Science, 274(6), 638-647.

Morse, J.W. & Mackenzie, F.T. (1990). Geochemistry of Sedimentary Carbonates. Developments in Sedimentology, 48. Elsevier, Amsterdam, 706 pp.

Morse, J. W., Andersson, A. J., & Mackenzie, F. T. (2006). Initial responses of carbonate-rich shelf sediments to rising atmospheric pCO_2 and "ocean acidification": Role of high Mg-calcites. Geochimica et Cosmochimica Acta, 70(23), 5814-5830.

Morse, J. W., Arvidson, R. S., & Lüttge, A. (2007). Calcium carbonate formation and dissolution. Chemical Reviews, 107(2), 342-381.

Mouret, A., Anschutz, P., Deflandre, B., Chaillou, G., Hyacinthe, C., Deborde, J., Etcheber, H., Jouanneau, J., Gremare, A., & Lecroart, P. (2010). Oxygen and organic carbon fluxes in sediments of the Bay of Biscay. Deep-Sea Research Part I: Oceanographic Research Papers, 57(4), 528-540.

Mucci, A. (1983). The solubility of calcite and aragonite in seawater at various salinities, temperatures, and one atmosphere total pressure. American Journal of Science, 283(7), 780-799.

Mucci, A., Canuel, R. & Zhong, S. (1989). The solubility of calcite and aragonite in sulfate-free seawater and the seeded growth kinetics and composition of the precipitates at 25°C. Chemical Geology, 74(3–4), 309-320.

Mucci, A., Sundby, B., Gehlen, M., Arakaki, T., Zhong, S., & Silverberg, N. (2000). The fate of carbon in continental shelf sediments of eastern Canada: a case study. Deep-Sea Research Part II: Topical Studies in Oceanography, 47(3), 733–760.

Mucci, A., Starr, M., Gilbert, D., & Sundby, B. (2011). Acidification of Lower St. Lawrence Estuary bottom waters. Atmosphere-Ocean, 49(3), 206–218.

Orr, J.C., Fabry, V.J., Aumont, O., Bopp, L., Doney, S.C., Feely, R.A., Gnanadesikan, A., Gruber, N., Ishida, A., Joos, F., Key, R.M., Lindsay, K., Maier-Reimer, E., Matear, R., Monfray, P., Mouchet, A., Najjar, R.G., Plattner, G.K., Rodgers, K.B., Sabine, C.L., Sarmiento, J.L., Schlitzer, R., Slater, R.D., Totterdell, I.J., Weiring, M.F., Yamanaka, Y., & Yool, A. (2005). Anthropogenic ocean acidification over the twenty-first century and its impact on calcifying organisms. Nature, 437, 681–686.

Orr, J.C. (2011). Recent and future changes in ocean carbonate chemistry. In: Gattuso, J.P., & Hansson, L. (Eds.), Ocean Acidification, 41-63. Oxford University Press, New York.

Orth, C. J., Gilmore, J. S., Quintana, L. R., & Sheehan, P. M. (1986). Terminal Ordovician extinction: Geochemical analysis of the Ordovician/Silurian boundary, Anticosti Island, Quebec. Geology, 14(5), 433-436.

Parker, L. M., Ross, P. M., O'Connor, W. A., Borysko, L., Raftos, D. A., & Pörtner, H.O. (2012). Adult exposure influences offspring response to ocean acidification in oysters. Global Change Biology, 18, 82–92.

Plante, S., Chabot, D., & Dutil, J. D. (1998). Hypoxia tolerance in Atlantic cod. Journal of Fish Biology, 53(6), 1342-1356.

Poole, R. & Tomczak, M. (1999). Optimum multiparameter analysis of the water mass structure in the Atlantic Ocean thermocline. Deep-Sea Research Part I: Oceanographic Research Papers, 46, 1895–1921

Rabalais, N. N., Turner, R. E., Justic, D., Dortch, Q., & Wiseman Jr, W. J. (1999). Characterization of hypoxia: topic I report for the integrated assessment on hypoxia in the Gulf of Mexico: NOAA Coastal Ocean Progam, Decision Analysis Series No. 15. NOAA Coastal Ocean Program, Silver Spring, 167 p.

Rabalais, N. N., Turner, R. E., & Wiseman, W. J. (2001). Hypoxia in the Gulf of Mexico. Journal of Environmental Quality, 30(2), 320-329.

Rabalais, N. N., Turner, R. E., & Wiseman Jr, W. J. (2002). Gulf of Mexico hypoxia, aka "The dead zone". Annual Review of Ecology and Systematics, 33(1), 235-263.

Raven, J. A., & Falkowski, P. G. (1999). Oceanic sinks for atmospheric CO_2. Plant, Cell & Environment, 22(6), 741-755.

Reddy, M. M. (1977). Crystallization of calcium carbonate in the presence of trace concentrations of phosphorus-containing anions. Journal of Crystal Growth, 41, 287-295.

Redfield, A. C., Ketchum, B. H., & Richards, F. A. (1963). The influence of organisms on the composition of seawater. In: Hill, M.N. (Eds.) The composition of seawater: Comparative and descriptive oceanography. The sea: ideas and observations on progress in the study of the seas, 2, 26-77.

Ries, J. B., Cohen, A.L. and McCorkle, D.C. (2009). Marine calcifiers exhibit mixed responses to CO_2-induced ocean acidification. Geology, 37, 1131-1134.

Sabine, C.L. & Feely, R.A. (2007). The oceanic sink for carbon dioxide. Greenhouse Gas Sinks. CABI Publishing, 31-49.

Sigman, D. M., & Boyle, E. A. (2000). Glacial/interglacial variations in atmospheric carbon dioxide. Nature, 407(6806), 859.

Silverberg, N., Bakker, J., Edenborn, H. M., & Sundby, B. (1987). Oxygen profiles and organic carbon fluxes in Laurentian Trough sediments. Netherlands Journal of Sea Research, 21(2), 95-105.

Sjöberg, E.L. (1978). Kinetics and mechanism of calcite dissolution in aqueous solutions at low temperatures. Stockholm Contributions in Geology, 32, 92.

Stanley, S. M., & Hardie, L. A. (1998). Secular oscillations in the carbonate mineralogy of reef-building and sediment-producing organisms driven by tectonically forced shifts in seawater chemistry. Palaeogeography, Palaeoclimatology, Palaeoecology, 144(1-2), 3-19.

Sternbeck, J., & Sohlenius, G. (1997). Authigenic sulfide and carbonate mineral formation in Holocene sediments of the Baltic Sea. Chemical Geology, 135(1-2), 55-73.

Stumm, W., & Morgan, J. J. (1996). Aquatic Chemistry: Chemical equilibria and rates in natural waters. Chichester: Wiley, New York, 1022 pp.

Sunda, W. G., & Cai, W. J. (2012). Eutrophication induced CO_2-acidification of subsurface coastal waters: Interactive Effects of temperature, salinity, and atmospheric pCO_2. Environmental Science & Technology, 46(19), 10651-10659.

Talmage, S. C., & Gobler, C. J. (2010). Effects of past, present, and future ocean carbon dioxide concentrations on the growth and survival of larval shellfish. Proceedings of the National Academy of Sciences, 107(40), 17246-17251.

Tans, P.P. & Keeling, R. (2016). Dr. Pieter Tans, NOAA/ESRL (www.esrl.noaa.gov/gmd/ccgg/trends/) and Dr. Ralph Keeling, Scripps Institution of Oceanography (scrippsco2.ucsd.edu/).

Terjesen, S. G., Erga, O., Thorsen, G., & Ve, A. (1961). Phase boundary processes as rate determining steps in reactions between solids and liquids: The inhibitory action of metal ions on the formation of calcium bicarbonate by the reaction of calcite with aqueous carbon dioxide. Chemical Engineering Science, 14(1), 277-288.

Thamdrup, B. (2000). Bacterial manganese and iron reduction in aquatic sediments. In: Bernhard. Schink (Ed.), Advances in Microbial Ecology. Advances in Microbial Ecology, 16, 41-84. Springer, Boston, MA.

Thibodeau, B., de Vernal, A. & Mucci, A. (2006) Recent eutrophication and consequent hypoxia in the bottom waters of the Lower St. Lawrence Estuary: Micropaleontological and geochemical evidence. Marine Geology, 231(1-4), 37-50.

Tucker, M. E., & Wright, V. P. (1990). Carbonate sedimentology. Blackwell Science Ltd, Malden, USA, 496 p.

United Nations, Department of Economic and Social Affairs, Population Division. (2017). World Population Prospects: The 2017 Revision, Key Findings and Advance Tables. Working Paper No. ESA/P/WP/248.

Veetil, S. P., Mucci, A., & Arakaki, T. (2018). Dolomite dissolution kinetics in aqueous solutions in the presence of organic and inorganic additives at 25° C and pCO_2~ 1 atm. Chemical Geology, 483, 98-110.

Walter, L. M., & Burton, E. A. (1990). Dissolution of recent platform carbonate sediments in marine pore fluids. American Journal of Science, 290(6), 601-643.

Wolf-Gladrow, D. A., Zeebe, R. E., Klaas, C., Körtzinger, A., & Dickson, A. G. (2007). Total alkalinity: The explicit conservative expression and its application to biogeochemical processes. Marine Chemistry, 106(1-2), 287-300.

Working Group on the State of the St. Lawrence Monitoring. Overview of the State of the St. Lawrence. (2014). St. Lawrence Action Plan. Environment Canada, Québec's Ministère du Développement durable, de l'Environnement et de la Lutte contre les changements climatiques), Québec's Ministère des Forêts, de la Faune et des Parcs, Parks Canada, Fisheries and Oceans Canada, and Stratégies Saint-Laurent. 52 p.

Zeebe, R. E., & Westbroek, P. (2003). A simple model for the $CaCO_3$ saturation state of the ocean: The "Strangelove," the "Neritan," and the "Cretan" Ocean. Geochemistry, Geophysics, Geosystems, 4(12). doi:10.1029/2003GC000538

Chapter 2: The Impact of Oxygen Depletion and the Concomitant Acidification of Bottom Waters on the Preservation of Detrital Carbonates in the Gulf of St. Lawrence

Abstract:

Over the past century, dissolved oxygen concentrations (DO) in the bottom waters of the Lower St. Lawrence Estuary (LSLE) and the Gulf have decreased dramatically and led to the development of persistent hypoxia ($[O_2]$ = <62.5μmol/L) in the LSLE. Oxygen depletion has been attributed primarily to changes in ocean circulation in the northwest Atlantic Ocean and an increase in the flux of organic matter to the seafloor. Accumulation of metabolic CO_2 in these waters has also resulted in their acidification and a decrease in pH (0.3-0.4 pH unit), commensurate to the variation expected for oceanic surface waters by the end of this century, thus, making this setting an excellent analogue for studies of ocean acidification and its ecological impacts. The decrease in bottom-water pH is accompanied by a decrease in the carbonate ion concentration and the saturation state of the waters with respect to both calcite and aragonite (Ω_C and Ω_A). Although the Laurentian Trough sediments are mostly devoid of modern calcium carbonate fossils, detrital (Ordovician/Silurian) carbonates originating from Anticosti Island accumulate on the neighboring seafloor. This study examines the impact of oxygen depletion and the concomitant acidification of bottom waters on the preservation of these detrital carbonates in the Laurentian Trough. Evidence of carbonate mineral dissolution is supported by an analysis of the inorganic carbon content of the sediments and their pore water chemistry. Historical data are used to determine the temporal evolution of the solid phase profiles as well as document spatial variations of preservation is examined. Finally, the mineralogy, chemical (Mg/Ca) and stable isotopic composition ($\delta^{13}C$ and $\delta^{18}O$) of carbonates in sediment cores recovered in the Trough were compared to the source material eroded from Anticosti Island.

2.1 – Introduction

Over the past 180 years, carbon dioxide (CO_2) concentrations in the atmosphere have increased exponentially, surpassing the 400 ppm mark at the end of 2014. These concentrations exceed pre-industrial levels by nearly 40% and surpass all levels recorded in the past 800,000 years (Feely et al., 2004; Doney et al., 2009; Feely et al., 2009; Le Quéré et al., 2009; Tans and Keeling, 2016). Since the onset of industrialization, the ocean, the largest CO_2 reservoir on Earth, has taken up just over a quarter of all anthropogenic emissions to the atmosphere making it the largest sink of anthropogenic CO_2 (Feely et al., 2004; Sabine and Feely, 2007; Feely et al., 2009; Gattuso and Hansson, 2011). The sequestration of anthropogenic CO_2 by the ocean prompts a decrease in pH, or ocean acidification (OA), which, over the past century has led to a decrease of ~0.1 in the pH of the surface ocean (Caldeira and Wickett, 2005). The Intergovernmental Panel on Climate Change (IPCC) "business as usual" scenario (IS592a) predicts that CO_2 concentrations will exceed 700 ppm by 2100 (IPCC, 2007). This, ultimately, will cause the pH of the surface ocean to decrease by another 0.3-0.4 unit by 2100, further lowering the saturation state of seawater with respect to calcium carbonate minerals ($CaCO_3$) (Orr et al., 2005; Orr, 2011). The saturation state is defined as:

$$\Omega_{C,A} = \frac{[Ca^{2+}][CO_3^{2-}]}{K^*_{sp}} \quad \textbf{(1)}$$

where [i] are total ion concentrations and K^*_{sp} is the stoichiometric solubility constant of calcite (C) or aragonite (A) under in-situ conditions (Mucci, 1983; Millero et al., 1995). Most of the surface ocean is currently supersaturated with respect to calcite and aragonite ($\Omega_{C,A}>1$) whereas the deep ocean is not. This is largely due to both calcium carbonate polymorphs displaying retrograde solubility (i.e., increasing solubility with decreasing temperature) and greater solubility with increasing pressure or, in this case, increasing depth in the water column. OA has raised the aragonite and calcite saturation depths (depth at which Ω_A and Ω_C are respectively equal to 1) and their respective compensation depths (depths at which no net accumulation of calcite or aragonite occurs) by 30-200 m from the pre-industrial to present (Feely et al., 2004; Doney et al., 2009; Feely et al., 2009) triggering the dissolution of $CaCO_3$ minerals and neutralizing some the anthropogenic CO_2 that has reached the deep ocean (Archer et al., 1998, Sulpis et al., 2018),

making carbonate-rich sediments the ultimate short-term sink of anthropogenic CO_2. The overall reaction describing the neutralization of anthropogenic CO_2 is:

$$CaCO_3 + CO_{2(aq)} + 2H_2O \rightleftharpoons 2HCO_3^- + Ca^{2+} \quad \textbf{(2)}$$

Coastal regions are especially vulnerable to acidification, making them the first environments to show the most profound consequences of this phenomena (Gattuso et al., 1998; Orr et al., 2005; Gattuso and Hansson, 2011). The coastal ocean is the most productive marine environment on Earth, accounting for almost 30% of all primary productivity in the ocean, despite comprising only 10% of its surface area (Gattuso et al., 1998; Gattuso and Hansson, 2011; Bauer et al., 2013). These highly productive environments are also commonly susceptible to eutrophication in response to the increased flux of nutrients from human activities and the consequent increase in organic matter (OM) production through photosynthesis and its export at depth (Berner and Berner, 1996; Gattuso and Hansson, 2011; Mackenzie et al., 2011). In a strongly stratified water column, where oxygen is not readily replenished at depth through advective mixing, the increased flux of particulate organic matter can lead to oxygen (O_2) depletion at depth upon the microbial degradation of the OM and the accumulation of metabolic CO_2. The latter greatly intensifies the effects of OA, beyond the contribution from the atmosphere (Cai et al., 2011; Gehlen et al., 2011; Mucci et al., 2011).

Most of the OM produced in the surface ocean undergoes microbial degradation as it settles through the water column and is remineralized back into CO_2. A fraction, however, makes it to the seafloor where it will sustain a suite of microbially-mediated diagenetic reactions that will alter the pore water chemistry, including their saturation state with respect to $CaCO_3$ minerals and preservation of the latter (Froelich et al., 1979; Mucci et al., 2000). Whereas $CaCO_3$ delivered to the seafloor may be dissolved during aerobic respiration of sedimentary organic matter, suboxic (Mn and Fe oxide reduction) and anoxic diagenesis (sulfate reduction and fermentation) may lead to authigenic carbonate mineral precipitation (Froelich et al., 1979; Gaillard et al., 1989; Boudreau et al., 1992; Mucci et al., 2000). Microbial degradation of organic matter (aerobic and anaerobic) in marine sediments also generates soluble reactive phosphate (SRP) and dissolved organic matter

(DOC), both of which can inhibit $CaCO_3$ dissolution and precipitation reactions and, thus, affect their preservation (Morse et al., 2007).

In this paper, we investigate the impacts of oxygen depletion and the concomitant acidification of bottom waters in the Laurentian Trough on the preservation of $CaCO_3$ minerals in Gulf of St. Lawrence sediments. We address these objectives from interpretations of the chemical and isotopic analyses of sediments and pore waters from box cores taken over the past ~15 years at three stations (17 (2010, 2014, 2016), 18 (2003, 2013, 2016) and Anticosti (2017)) in the Gulf of St. Lawrence, in proximity to Anticosti Island.

2.2 – Geological Setting

The St. Lawrence Estuary (SLE) is the largest enclosed estuary in the world. It is located in Eastern Canada and links the Great Lakes through the St. Lawrence River to the North Atlantic Ocean (see Figure 2.1). The true estuary starts at the eastern tip of Ile d'Orléans (i.e., first intrusion of seawater), a few kilometers east of Quebec City, and is typically described by three major segments: the Upper St. Lawrence Estuary (USLE), from Ile d'Orléans to Tadoussac, the Lower St. Lawrence Estuary (LSLE), from Tadoussac to Pointe-des-Monts and the Gulf of St. Lawrence (GSL). The Gulf of St. Lawrence is a partially enclosed sea, which is connected to the North Atlantic Ocean through the Cabot Strait and the Strait of Belle Isle. The dominant morphological feature of the estuary is the Laurentian Trough, a 1240 km long, 300-600 m deep, submarine canyon, that extends from the continental shelf break westward to the head of the LSLE at Tadoussac. The sediments within the Trough are composed of, on average, 60% clay, 35% silt, and 5% sand. They are primarily derived from the mechanical weathering of Precambrian silicate shield rocks to the north and the Early Palaeozoic sedimentary rocks of the Appalachians to the south (Nota and Loring, 1964; Piper et al., 1990; Jaegle, 2015). These sediments are almost completely devoid of $CaCO_3$ minerals, apart from the accumulation of detrital $CaCO_3$ on the seafloor around Anticosti Island - a 222 km long and 56 km wide Ordovician-Silurian Carbonate Platform (Desrochers, 2006; Desrochers et al., 2010; James et al., 2015). Over the past century, the combination of warmer bottom waters, changes in the mixing ratio of source-water masses at the shelf edge and microbial degradation of organic matter settling from the surface has led to the

depletion of oxygen and the accumulation of metabolic CO_2 within the bottom waters of the GSL and LSLE, their acidification and the development of hypoxia in the LSLE (Gilbert et al., 2005; Mucci et al., 2011).

2.3 – Methods

2.31 – Sampling

In May 2016, sediment and pore water samples were recovered onboard the R/V Coriolis II at Stations 17 and 18 in the Laurentian Trough within the Gulf of the St. Lawrence (see Figure 2.1). These two stations were cored in previous years (17 - 2010 and 2014 and 18 - 2003 and 2013), providing historical data and additional material for analysis. In June 2017, additional sediment and pore water samples were retrieved, this time from Station Anticosti, ~40 kilometers south of Anticosti Island (see Table 2.1). On the same occasion, a sediment grab was taken from the delta of the Jupiter River on Anticosti Island (49°28'42"N 63°37'00"W) to retrieve carbonate samples from one of the tributary sources of the detrital material.

Undisturbed sediment cores were retrieved with an Ocean Instrument Mark II box corer. Immediately after a core (0.12 m^2 x 50 cm long) was recovered, it was transferred into a specially-designed Plexiglas glove box (Edenborn et al., 1986) where the atmosphere was purged and replaced by a steady flow of N_2 to limit redox reactions during sampling. Once in place, each core was sub-sampled at specific depth intervals; at 0.5-cm increments for the first centimeter, at 1-cm increments to 5 cm, at 2-cm increments to 15 cm, at 3-cm increments to 24 cm, and finally at 4-cm increments to 36 cm. At each depth interval, as the sediment was exposed by step-wise lowering of the front plate, sediment samples were transferred and stored in pre-weighed plastic vials. The vials were later weighed, freeze-dried, and re-weighed to determine the sediment water content. Sediment porosity was calculated (see Table 2.2a-g) from the water content and the salinity of the overlying seawater, as recorded by a SeaBird SBE-911 conductivity-temperature-depth (CTD) probe mounted on a rosette sampler that was lowered to within 5 meters of the bottom, using a dry sediment density of 2.65 g/cc. The water samples collected by Niskin bottles mounted on the rosette were analyzed for various parameters (pH_T, Total Alkalinity (TA),

Dissolved Silica (DSi), Soluble Reactive Phosphate (SRP)) allowing for the chemical characterization of the overlying waters (OLW) at each station. The analytical protocols are described in detail below. The freeze-dried sediments were then ground and homogenized with an agate pestle and mortar in preparation for later analyses. In addition, at each depth interval within the core, a portion of the sediment was transferred into Reeburgh-type squeezers (Reeburgh, 1967) and pore waters extracted (250-400 kPa N_2) as they were filtered through a 1 μm nominal pore size microfiber glass filter and 0.45 μm Millipore HA mixed cellulose filter into pre-washed polyethylene syringes. The collected pore waters were then rationed into two different bottles. A first portion was transferred into 30 mL, acid-washed, polyethylene bottles, and subsequently acidified with 1% by volume of concentrated trace metal-free HNO_3. A second portion was transferred into 30 mL amber glass bottles and poisoned with a few crystals of $HgCl_2$. All pore waters were kept refrigerated until analysis.

2.32 – Analyses

2.321 – Pore water and Overlying Waters

The total dissolved Ca, Fe and Mn concentrations of the acidified pore water samples were determined by flame atomic absorption spectrophotometry (AAS). Calibration curves were constructed using commercial, aqueous 1000 mg/L certified standard solutions. The detection limits for both Mn and Fe were 0.1 mg/L and 0.01mg/L for Ca. Reproducibility for these analyses was better than ±5%. pH, on the total proton concentration scale (pH_T), was determined onboard spectrophotometrically at 25.0°C using a m-cresol purple indicator solution with a precision of ±0.005 (Clayton and Byrne, 1993; Mucci et al., 2011). Total alkalinity was determined at the land-based laboratory by open-cell automated potentiometric titration (Titrilab 865, Radiometer®) with a pH combination electrode (pHC2001, Red Rod®) and a dilute (~0.01 N) HCl titrant. The latter was calibrated against Certified Reference Materials (CRM Batch#94, provided by A. G. Dickson, Scripps Institute of Oceanography, La Jolla, USA). Samples were drawn from the 30 mL $HgCl_2$-poisoned sample bottles and weighed on an analytical balance to ± 0.1 mg. The average relative error, based on the average relative standard deviation on replicate standard and sample analyses, was better than 0.15%.

The Dissolved Inorganic Carbon (DIC) concentration of the pore waters, extracted from the 2017 Anticosti core and stored in $HgCl_2$-poisoned bottles, was measured at the Laboratoire des Sciences du Climat et de l'Environnement in Gif-sur-Yvette (France) using a SciTech Apollo DIC analyzer. Once thermally equilibrated at 25°C, 1-1.5 mL of the sample was acidified with 10% H_3PO_4 after being injected into the instrument's reactor. The evolved CO_2 was carried to a LI-COR infrared analyzer by a stream of pure nitrogen. A calibration curve was constructed using gravimetrically prepared Na_2CO_3 solutions, and the accuracy of the measurements was verified using a CRM. Reproducibility was typically on the order of 0.2%.

Soluble Reactive Phosphate (SRP) and Dissolved Silica (DSi) concentrations were determined spectrophotometrically using, respectively, the phospho-molybdate and molybdate blue methods described in Grasshoff et al. (1999) in 10-cm and 1-cm pathlength cells. Calibration curves were constructed using dilutions of an in-house concentrated stock solution prepared gravimetrically with dried, anhydrous potassium dihydrogen and dilution of a commercial (Fisher Scientific), 1000 ppm Si atomic absorption standard solution. The detection limit was 0.01 µmol/L for both SRP and DSi while the precision was ~±5%.

The $\partial^{13}C$ (DIC) of the pore waters extracted from sediments recovered at Station 18 (2016) and Anticosti (2017) were determined at the GEOTOP Stable Isotope Laboratory (Université du Québec à Montréal). Twelve drops of 100% phosphoric acid (H_3PO_4) were transferred to 3 mL glass vials and purged with helium. A few milliliters of the pore waters were injected with a syringe through the septum. The evolved, headspace CO_2 was sampled using a Micromass MicroGas^{TM} system and analyzed in continuous flow mode using an Isoprime 100^{TM} Isotope Ratio Mass Spectrometer (IRMS). Carbon isotopic values are reported in per mil (‰) with respect to Vienna PeeDee Belemnite (VPDB) referenced to the NBS19-LSVEC scale. Results were normalized on the NBS19-LSVEC scale using two internal reference materials ($\delta^{13}C$=-3.41‰ and -19.51‰ vs VPDB). Replicate $\delta^{13}C_{DIC}$ measurements of the same samples yielded a combined uncertainty of better than ±0.2‰ (1σ).

2.322 – Sediment

The Total Inorganic Carbon (TIC) content of the sediments was determined using a UIC Coulometrics™ coulometer following acidification of a weighed aliquot of the freeze-dried, ground and homogenized samples and CO_2 extraction. The detection range is between 1µg and 10,000 µg of carbon with a precision of ±2%. Contribution to TIC from pore water DIC precipitated during freeze drying was calculated and found to be negligible (<0.01%). Total Carbon (TC) was determined on the freeze-dried sediment samples using a Carlo Erba™ NC 2500 elemental analyzer (NC2500TM). Total Organic Carbon (TOC) was determined by subtracting TIC from TC (TOC=TC-TIC).

The stable carbon ($\partial^{13}C$) and oxygen ($\partial^{18}O$) isotope composition of the sedimentary $CaCO_3$ were analyzed on a gas-source mass spectrometer (Nu Instruments Perspective with NuCarb at McGill University). Phosphoric acid was added to sediment samples at 70°C, and the isotopic composition of the evolved CO_2 was used to determine the stable isotope signature, which was corrected with an acid fractionation factor of 1.00871, as calculated from Kim et al. (2007). Precision for $\partial^{13}C$ and $\partial^{18}O$ were <0.06‰ and <0.08‰ respectively. Carbon and oxygen isotopic values are reported in per mil (‰) with respect to Vienna PeeDee Belemnite (VPDB).

The carbonate mineralogy of sediment samples was determined by X-Ray diffraction spectrometry (Rigaku Smartlab™ X-Ray Diffractometer). Diffractograms were obtained using a copper cathode at 60kV and scanned over a 2ø range of 10º-60º at a scan rate of 1.5 º/minute. The cell volume value at the (104) peak was plotted against a calibration curve constructed with parameters taken from Bischoff et al. (1983) for biogenic calcites to determine the $MgCO_3$ modal content of the solid carbonate. The lower detection limit of this method is 0.4 $MgCO_3$% with an accuracy of 0.8 mol % (Titschack et al., 2011).

2.33 – Calculation of Carbonate Parameters

The calcite saturation state ($\Omega_{Calcite}$; see Equation 1) and DIC speciation of the overlying and pore waters were calculated using two of the three measured carbonate parameters: pH_T, DIC

and TA. According to Orr et al. (2018), the combined propagated uncertainty of pairing TA-DIC parameters is the lowest when attempting to calculate the carbonate ion concentration and therefore the saturation state. The carbonic acid dissociation constants of Mehrbach et al. (1973), refit by Dickson and Millero (1987), and the HSO_4^- constant of Dickson (1990) were used along with measured input variables, including SRP and DSi, in CO2SYS for the calculation of the in-situ pH_T and saturation state (Lewis and Wallace, 1998).

2.4 – Results

Location of sampling sites, their respective sampling month/year and selected bottom-water characteristics/properties (depth (m), T (ºC), S, pH_T and $\Omega_{Calcite}$) are presented in Table 2.1. All sediments retrieved from the trough are composed of fine silt-sized particles. Sedimentation rates in the Gulf of St. Lawrence to the south-west of Anticosti Island and the central Laurentian Channel/Trough were estimated by Smith and Schafer (1999) and later confirmed by Genovesi et al. (2011), using ^{210}Pb radiometric dating, to be 0.13 cm/year at Station 17 and 0.18 cm/year at Station 18.

The inorganic carbon (IC) content of the sediments at Station 18 (2013 and 2016) is relatively constant at depth but decreases sharply towards the sediment-water interface (SWI) (see Figure 2.2). Assuming that the rate of detrital carbonate delivery to the seafloor has been invariant over the time interval represented by at least the first 15 cm of our cores (~83 years at Station 18 and 115 years at Station 17), we estimated the amount of $CaCO_3$ dissolution, by integrating the loss of IC over the first 8 cm (1x1x8 cm) of the sediment, using the average, historical IC content at depth as the baseline. The integration was carried out over the first 8 cm since the IC content of the sediment is nearly constant below this depth, marking the vertical extent of dissolution. A dry sediment density of 2.65g/cm^3 and the calculated porosity were used in conjunction with the integrated area to calculate the amount of $CaCO_3$ dissolved, yielding 4.07, 4.36 and 5.72 μmol/cm^2 for 2003, 2013 and 2016, respectively. At Station Anticosti (2017), the vertical profile is similar and shows a gradual decrease in IC towards the SWI (see Table 2.2a-g). Using the same integration technique over the first 8 cm of sediment, we determined that 19.4 μmol/cm^2 has dissolved relative to the baseline IC content at depth. At Station 17 (2010, 2014 and 2016), the vertical IC profiles

are relatively uniform throughout the core, with the exception of positive excursions/anomalies within the 2014 and 2016 cores (see Table 2.2a-g).

X-ray diffraction (XRD) was used to determine the mineralogy of the sedimentary carbonates and differentiate between $CaCO_3$ polymorphs. Results indicate that calcite was the only calcium carbonate polymorph present in all cores. XRD analysis also confirmed that all carbonate minerals within the studied cores and from source rock were low magnesian calcites (<2.2 $\%MgCO_3$) (Bischoff et al., 1983; Titschack et al., 2011). The median $MgCO_3$ content of the calcite in the source material and at Stations 18 (2016), 17 (2016), and Anticosti (2017) were 0.88%, 0.80%, 0.50%, and 1.13% respectively. The organic carbon content (1.44-1.73 weight % at Station 18 (2016), 0.61-1.72 weight % at Station 17 (2016) and 0.33-1.61 weight % at Station Anticosti (2017)) of the sediments generally decreases smoothly with depth at all sampling sites (see Table 2.2a-g).

Pore water pH_T decreases abruptly below the SWI but recovers and eventually stabilizes with depth. This pattern mirrors that of the calcite saturation state ($\Omega_{Calcite}$), which also sharply decreases below the SWI but increases with depth (see Table 2.2a-g). Pore water calcium concentrations at Station 18 (2016) and Station Anticosti (2017) increase below the SWI before decreasing steadily with depth. In contrast, at Station 17 (2014), pore water calcium concentrations gradually decrease below the SWI (see Table 2.2a-g). The dissimilatory reduction of metal oxides (Mn(III) and Fe(III)) occurs immediately below the oxic zone where increased concentrations of pore water Mn(II) and Fe(II) are observed (see Table 2.2a-g). Total alkalinity (TA) and Dissolved Inorganic Carbon (DIC) concentrations generally increase consistently with depth in each core. Soluble Reactive Phosphate (SRP) concentrations increase with depth at Station 18 (2016) but, at Station Anticosti (2017), after an initial increase with depth, they sharply decrease below 15 cm depth (see Table 2.2a-g). Dissolved Silica (DSi) concentrations increased substantially immediately below the SWI and were relatively invariant for the remainder of the profile.

2.5 – Discussion

The accumulation and preservation of detrital $CaCO_3$ in the sediments of the Gulf of St. Lawrence varies both spatially and temporally. Accumulation of Inorganic Carbon varies with proximity to Anticosti Island, with the highest concentrations at Station Anticosti (the closest station to the island) and accumulation decreasing into the trough (see Figure 2.3). The fate of detrital $CaCO_3$ and evidence of its dissolution in response to bottom-water acidification in the Gulf of St. Lawrence sediments is explored by examining the temporal evolution of solid-phase and pore water profiles at the three stations near Anticosti Island. Sedimentation rates are quite low within the central Gulf and Laurentian Trough and were estimated at 0.13 cm/year at Station 17 and 0.18 cm/year at Station 18 (Smith and Schafer, 1999; Genovesi et al., 2011). Despite the progressive oxygen depletion and concomitant acidification of the overlying waters over the past century, unlike the LSLE, the water column and overlying waters in the study area remain supersaturated with respect to calcite ($\Omega_C>1$). Therefore, we can expect most of the detrital $CaCO_3$ supplied from Anticosti Island to survive the journey through the water column to the seafloor, allowing us to assume a constant supply of $CaCO_3$ to the sediment over time (i.e., steady state), at least over the period represented by the recovered cores. Available historical data of the OLW carbonate chemistry at Station 18 suggest that $\Omega_{Calcite}$ has decreased substantially from 2006 to 2016 at Station 18 (1.83 to 1.36) but has remained relatively stable from 2013 to 2016, fluctuating only slightly in response to the expansion and contraction of the O_2/pH minimum zone (Gilbert et al., 2005). In contrast, the $\Omega_{Calcite}$ at Station 17 has remained stable between 2010 and 2016 (see Table 2.1). Ultimately, as acidification amplifies and these bottom waters become less saturated with respect to calcite, less metabolic CO_2 production, resulting from oxic diagenesis of sedimentary organic matter, will be required to generate an undersaturation in the pore waters and trigger $CaCO_3$ dissolution in the oxic layer of the sediment.

The most compelling evidence of $CaCO_3$ dissolution in the sediment can be seen from the Inorganic Carbon (IC) profiles at Stations 18 (2016) and Anticosti (2017). The IC content of the sediment is constant (steady state) at depth but decreases progressively as the sediment-water interface (SWI) is approached (see Figure 2.2). At Station 18 (2016), this equates to a 24% decrease in IC abundance within the first centimeter. Likewise, at Station Anticosti (2017), the IC

content is nearly invariant at depth, with the exception of a couple deviations (likely due to the presence of shells), but increases towards the SWI, indicating loss of IC at or close to the SWI (see Figure 2.4). Dissolution was quantified through the integration of the amount of $CaCO_3$ lost to dissolution in relation to the steady-state concentration at depth. Results indicate that at Station 18 (2016), 5.72 μmol/cm^2 of $CaCO_3$ dissolved over the first 8 cm (1x1x8cm). Likewise, 19.4 μmol/cm^2 has been dissolved at Station Anticosti (2017) over the same depth interval.

Evidence of sedimentary $CaCO_3$ dissolution can also be observed in the pore waters within the top 1 cm at Station 18 (2016), which coincides with the Oxygen Penetration Depth (OPD) in these sediments (Silverberg et al., 2000), as further supported by the initiation of Mn(III)/Fe(III) oxide reduction and the accumulation of pore water Mn(II)/Fe(II) below this depth (see Table 2.2a-g). The oxic degradation of organic matter leads to the accumulation of metabolic CO_2 in sediment pore waters, which in turn, leads to the release of protons (H^+) and ultimately a decrease in pH (Mucci et al., 2000). Assuming that the composition of organic matter can be represented by the Redfield stoichiometry (Redfield et al., 1963), the suite of diagenetic reactions in marine sediments and their effects on A_C, pH and Ω are outlined in Table 2.3.

Accordingly, the outcome of oxic degradation of organic matter can be observed by a sudden drop in pH immediately (within the first centimeter) below the sediment-water interface (SWI). Pore water pH, however, increases with depth below the oxic layer as the remineralization of OM proceeds by Mn(III)/Fe(III) oxide reduction (see Table 2.2a-g and Table 2.3). The overlying waters (OLW) at Station 18 are supersaturated with respect to calcite (Ω_C = 1.36; see Table 2.2a-g), but the pH decrease induced by the oxic respiration of OM drives the $\Omega_{Calcite}$ below saturation (Ω_C =0.86) (see Figure 2.5; see Table 2.2a-g). The drop in $\Omega_{Calcite}$ below saturation within the first centimeter of the sediment should trigger the dissolution of the detrital carbonates reaching the seafloor and buried immediately below the sediment-water interface (see Table 2.2a-g). Clear evidence of $CaCO_3$ dissolution is observed from the increased pore water calcium concentration immediately below the SWI (relative to the OLW whose [Ca^{2+}] can be calculated from their salinity to be 10.21 mmol/kg; see Table 2.1). At Station 18 (2016), pore water calcium concentrations increase by ~3.4% within the first cm below the SWI, (10.21 to 10.56 mmol/kg; see Figure 2.5; see Table 2.2a-g) but gradually decrease with depth as authigenic $CaCO_3$

precipitation occurs in response to alkalinity production following suboxic and anoxic degradation of sedimentary organic matter. The pore water calcium concentration is positively correlated to the IC content and negatively to $\Omega_{Calcite}$ below the SWI ($p=0.00559$), strongly suggesting that $CaCO_3$ dissolution is occurring just below the SWI.

Although significant detrital calcite dissolution occurs at Station 18, a comparison of the IC profiles from 2003, 2013 and 2016 reveals that diagenetically-driven dissolution of sedimentary IC in the oxic zone at this station has increased over at least the past decade (see Figure 2.2). Dissolution is evident in 2013 and 2016 from the presence of a negative spike in IC content (relative to the surface) immediately below the SWI, but this excursion is not observed in 2003. The lack of evidence of calcite dissolution at the surface of the core recovered in 2003 may be due to the loss of the first few millimeters of the core during sampling. To determine the amount of detrital $CaCO_3$ lost through dissolution in each core, we integrated to a depth of 8 cm (the vertical extent of dissolution), using the historical record at depth of the steady-state $CaCO_3$ accumulation rate. The results (2003 - 4.07 $\mu mol/cm^2$, 2013 - 4.36 $\mu mol/cm^2$; 2016 - 5.72 $\mu mol/cm^2$) clearly show the progressive dissolution of $CaCO_3$ over the last 13 years. This phenomenon is even more striking when we limit the integration to the first centimeter (oxic layer): 1.66 $\mu mol/cm^2$ in 2003 and 3.19 $\mu mol/cm^2$ in 2016. These values also reflect an increase in dissolution rate from 0.30 $\mu mol/cm^2$/year in 2003 to 0.58 $\mu mol/cm^2$/year in 2016. The overall increase (~93%) between 2003 and 2016 in dissolution rate translates into a significant decrease in the preservation of $CaCO_3$ during this time. This confirms that active dissolution at this station has increased in magnitude and rate over the span of 13 years. Evidence of $CaCO_3$ dissolution in these sediments was present in 2003, but by 2013 it had further developed and by 2016 it had greatly intensified ($p=0.00296$). Hence, $CaCO_3$ dissolution (burn-down) at Station 18 has accelerated between 2003 and 2016.

Evidence of $CaCO_3$ dissolution in the first 1.5 cm centimeters of sediment can also be observed from the pore water profile at Station Anticosti (2017), but unlike at Station 18, active $CaCO_3$ dissolution appears to extend to 1.5 cm depth, as the OPD appears to be deeper. This is to be expected because of the lower OC content (0.33-1.61 wt%) of the sediment at this station. Below the SWI, pH decreases but recovers quickly with depth as Mn(III)/Fe(III) oxide reduction intensifies. The overlying waters (OLW) at Station Anticosti are also supersaturated with respect

to calcite (Ω_C = 1.29; see Table 2.2a-g), but oxic respiration of OM drives down the pH and the $\Omega_{Calcite}$ well below saturation (Ω_C =0.81) by 1.5 cm depth (see Figure 2.4; see Table 2.2a-g) and triggers the dissolution of the detrital carbonates buried below the sediment-water interface at this site (see Table 2.2a-g). Like at Station 18, a pore water calcium gradient provides evidence of active $CaCO_3$ dissolution, as calcium concentrations increase by ~11.1% relative to the OLW within the first 1.5 cm of the core below the SWI (10.20 to 11.33 mmol/kg see Figure 2.4; see Table 2.2a-g) but gradually decrease with depth as authigenic $CaCO_3$ precipitates during suboxic and anoxic diagenesis. Like at Station 18, the pore water calcium concentrations at Station Anticosti are positively correlated to $\Omega_{Calcite}$ and negatively correlated to the IC content below the SWI ($p=0.0220$), evidence that $CaCO_3$ dissolution occurs below the SWI. Curiously, pore water Soluble Reactive Phosphate (SRP) concentrations do not increase throughout this core as they do at Station 18. Instead, SRP steadily increases to a depth of ~15 cm then its concentration decreases sharply, suggesting that it is adsorbing to the surface of sedimentary carbonates, which are three times more abundant at Station Anticosti than at the two other stations investigated in this study (Berner and Morse, 1974; Reddy, 1977; Millero et al., 2001). The lower range of SRP concentrations could also be attributed to the lower OM content of these sediments, the source of pore water SRP, at Station Anticosti (0.33-1.61 weight % OC) in comparison to Station 18 (1.44-1.73 weight % OC).

Even though there is clear evidence of $CaCO_3$ dissolution in the oxic layer of the sediments at Stations 18 and Anticosti, it is undiscernible at Station 17. Box cores taken at Station 17 in 2010, 2014 and 2016 and the IC profiles show no evidence of ongoing dissolution (see Figure 2.6), as the IC content of the sediment is relatively uniform throughout the cores except for positive deviations in 2014 and 2016 which are likely attributable to adventitious $CaCO_3$ hard parts (mollusk shells). Located closer to the Cabot Strait, the OLW at Station 17 are slightly more supersaturated than at the other sampled stations ($\Omega_{Calcite}$ = 1.48 (2016), 1.62 (2014) and 1.46 (2010)), thus requiring the production of more metabolic CO_2 to generate a pore water undersaturation in the oxic layer of the sediment. The OC content of the sediment at Station 17 is also slightly less (0.61-1.72 weight % OC) than at Station 18 (1.44-1.73 weight % OC), as is the sedimentation rate (0.13 vs 0.18 cm/year). This likely decreases the sediment oxidant demand and rate of oxic diagenesis and metabolic CO_2 production relative to the two other stations. On the

basis of the IC profiles alone, we cannot discern dissolution of $CaCO_3$ in the sediments at Station 17 yet, but it should develop in the future upon further acidification of the OLW.

No significant variation was found (18 - p=0.9151, 17 - p=0.8765, Anticosti - p=0.9368) between the $MgCO_3$ content of the source material and the carbonate minerals preserved in the sediments (see Figure 2.7). The stable oxygen and carbon isotope compositions ($\partial^{13}C$ & $\partial^{18}O$ VPDB) of the source rocks and sedimentary carbonate minerals recovered at the three study sites were also compared and significant differences were found (all $p<0.00001$; see Figure 2.8). However, the $\partial^{13}C$ (VPDB) signatures are generally more stable than the $\partial^{18}O$, as they are expected to alter or reset long after the latter and only upon recrystallization of the original material (Ahm et al., 2018). The $\partial^{18}O$ (VPDB) signature of the source material is notably depleted in ^{18}O (relative to modern seawater), likely because they were precipitated during a global greenhouse period (Ordovician and Silurian) when the ocean had a large glacial meltwater component (Desrochers, 2006; James et al., 2015). Carbonate minerals preserved in the sediments recovered at the three stations within the Laurentian Trough are enriched in ^{18}O relative to the source material. The enrichment may reflect the preferential dissolution of the light isotope (^{16}O) and enrichment in the heavier isotope (^{18}O) detrital material during early diagenesis (Bickert, 2006). More likely, the stable oxygen isotopic composition of these carbonates was reset to near modern values by isotope exchange as the fine grained material settled through the water column and accumulated in the sediment (Ahm et al., 2018). Even though it is not as pronounced, there is a significant difference in the $\partial^{13}C$ signature of the source rock and the carbonate minerals in sediments recovered from the Trough. Given that the $\partial^{13}C$ signature of the source rock is not expected to be reset as fast as the $\partial^{18}O$ signature (Ahm et al., 2018), this discrepancy likely reflects remineralization of $CaCO_3$ below the SWI from pore waters in which lighter DIC has accumulated upon the microbial degradation of organic matter (Bickert, 2006).

2.6 – Summary and Conclusions

With the exception of Station 17, the seaward-most station visited in this study, the preservation of detrital carbonates within the Gulf of St. Lawrence sediments has been greatly affected by the recent oxygen depletion and its concomitant acidification of the bottom waters.

The acidification of the bottom waters within the Trough to the south-west of Anticosti Island has caused their saturation state ($\Omega_{Calcite}$) to decrease enough that the production of metabolic CO_2 within the oxic zone of the sediment, immediately below the sediment-water interface (SWI), is now sufficient to generate calcite-undersaturated pore waters and trigger the dissolution of $CaCO_3$ particles that reach the seafloor. This is clearly reflected in variations of the IC content of the sediments below the SWI at Station 18 and Station Anticosti where the lost $CaCO_3$ through dissolution over the first 8 cm (1x1x8cm) amounts to 5.72 μmol/cm^2 and 19.4 μmol/cm^2 respectively. Likewise, pore water calcium concentrations increase significantly at both stations immediately below the SWI, complementing the sharp decrease in IC below the surface. Based on the available multi-year data, we can conclude that the amount and rate (+93%) of dissolution of $CaCO_3$ minerals has intensified at Station 18 between 2003 and 2016. The increased dissolution rate is the result of a notable drop in the $\Omega_{Calcite}$ (1.83 to 1.36) of the OLW between 2005 to 2016, allowing the production of metabolic CO_2 in the pore waters to further amplify the undersaturation that develops within the oxic layer of the sediment and drive greater calcite dissolution. Finally, seaward of the latter two stations, at Station 17, evidence of $CaCO_3$ dissolution could not yet be discerned, as the saturation state of the OLW at this station ($\Omega_{Calcite}$ = 1.46-1.62) is higher and the production of metabolic CO_2 in the oxic zone of the sediment is lower given the slightly lower organic carbon accumulation rate.

2.7 Acknowledgements

We would like to thank the Department of Fisheries and Oceans (DFO) for financial support of this project through the SECO.Net Grant. We wish to acknowledge Jens Rassmann and Bruno Bombled for measuring the DIC concentrations on the pore waters recovered from the Station Anticosti (2017) core. We would like to thank Dr. Thi Hao Bui for performing the stable oxygen and carbon isotope analyses on all the sediment samples and Dr. Jean-Francois Hélie for carrying out the $\partial^{13}C$(DIC) measurements on sediment pore waters. We wish to acknowledge Constance Guignard for her time and support in the laboratory. Finally, we would like to give special thanks to Gilles Desmeules as well as the Captains and crew of the R/V Coriolis II without whom, over the years, this project would not have been possible.

Figure 2.1: Map of the St. Lawrence Estuary and Gulf, Upper St. Lawrence Estuary (USLE), Lower St. Lawrence Estuary (LSLE) and Gulf of St. Lawrence (GSL). Stations 17, 18 and Anticosti are also indicated.

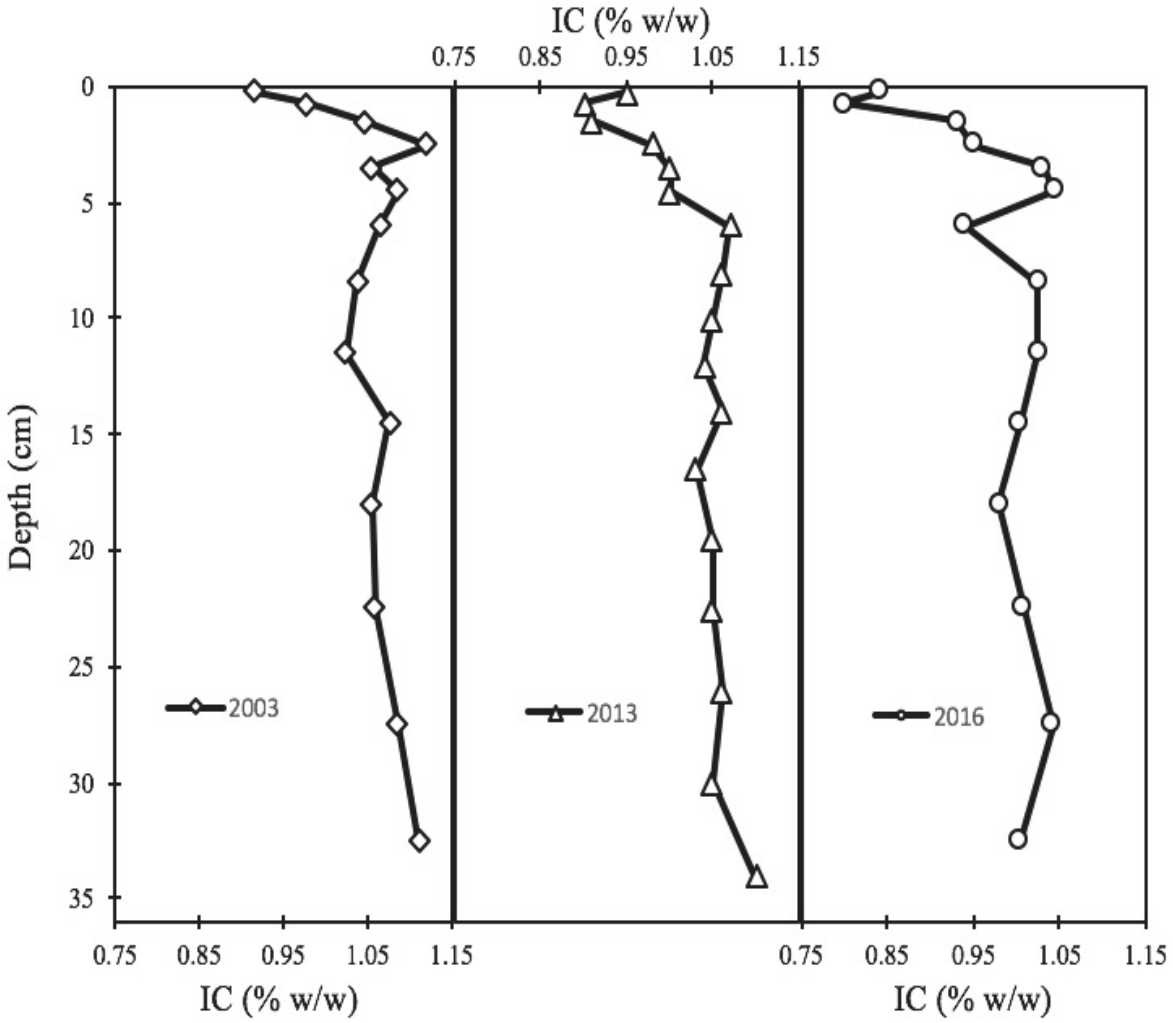

Figure 2.2: Inorganic carbon (IC) vertical profiles at Station 18 for the years 2003, 2013 and 2016. The amount of $CaCO_3$ lost to dissolution was calculated (to 8 cm depth, 1 cm x1 cm x 8 cm) to be: 2003 - 4.07 μmol/cm^2, 2013 - 4.36 μmol/cm^2, 2016 - 5.72 μmol/cm^2.

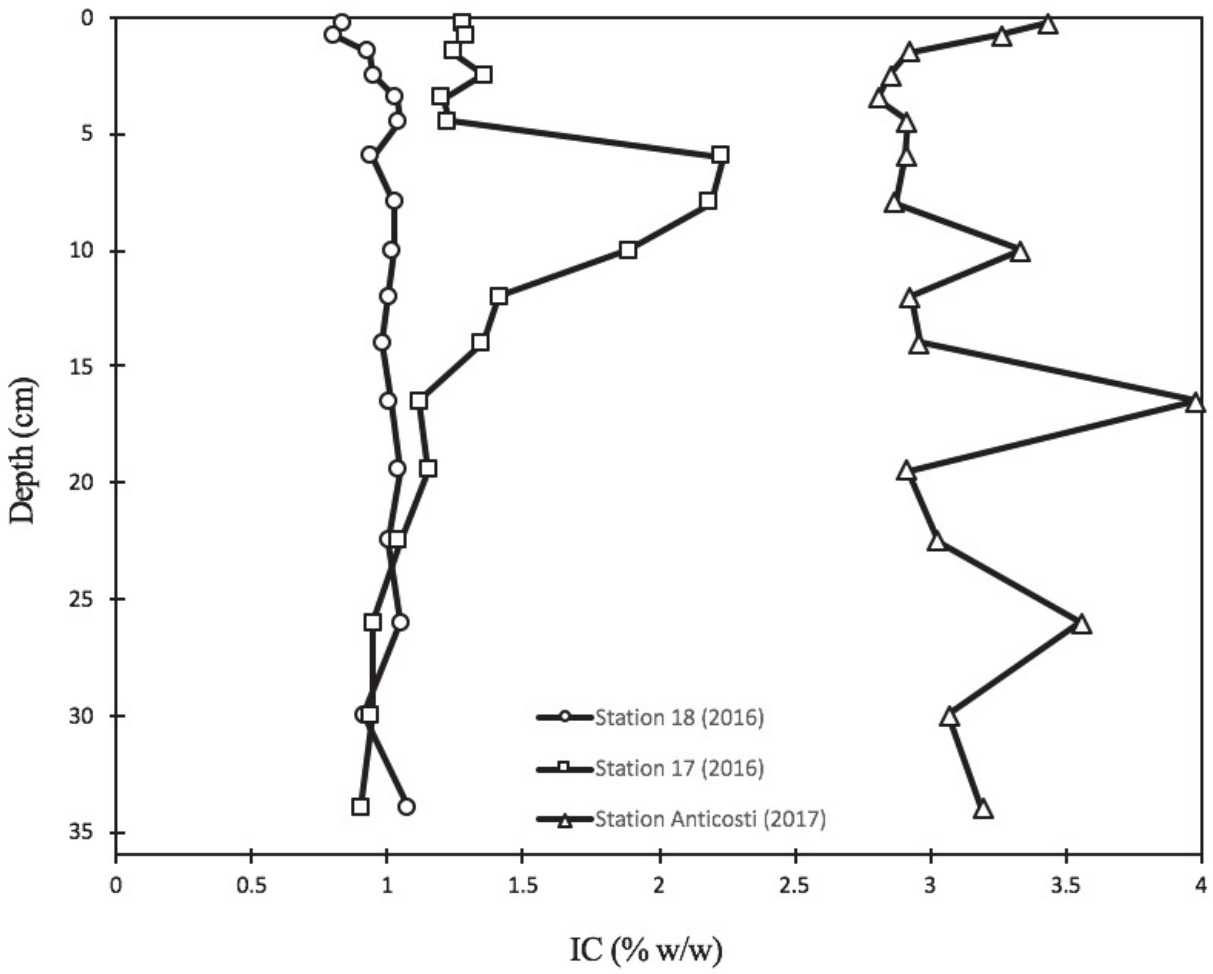

Figure 2.3: Inorganic carbon (IC) vertical profiles showing variations in $CaCO_3$ accumulation within the Gulf of St. Lawrence sediments. Concentrations decrease with distance from the island.

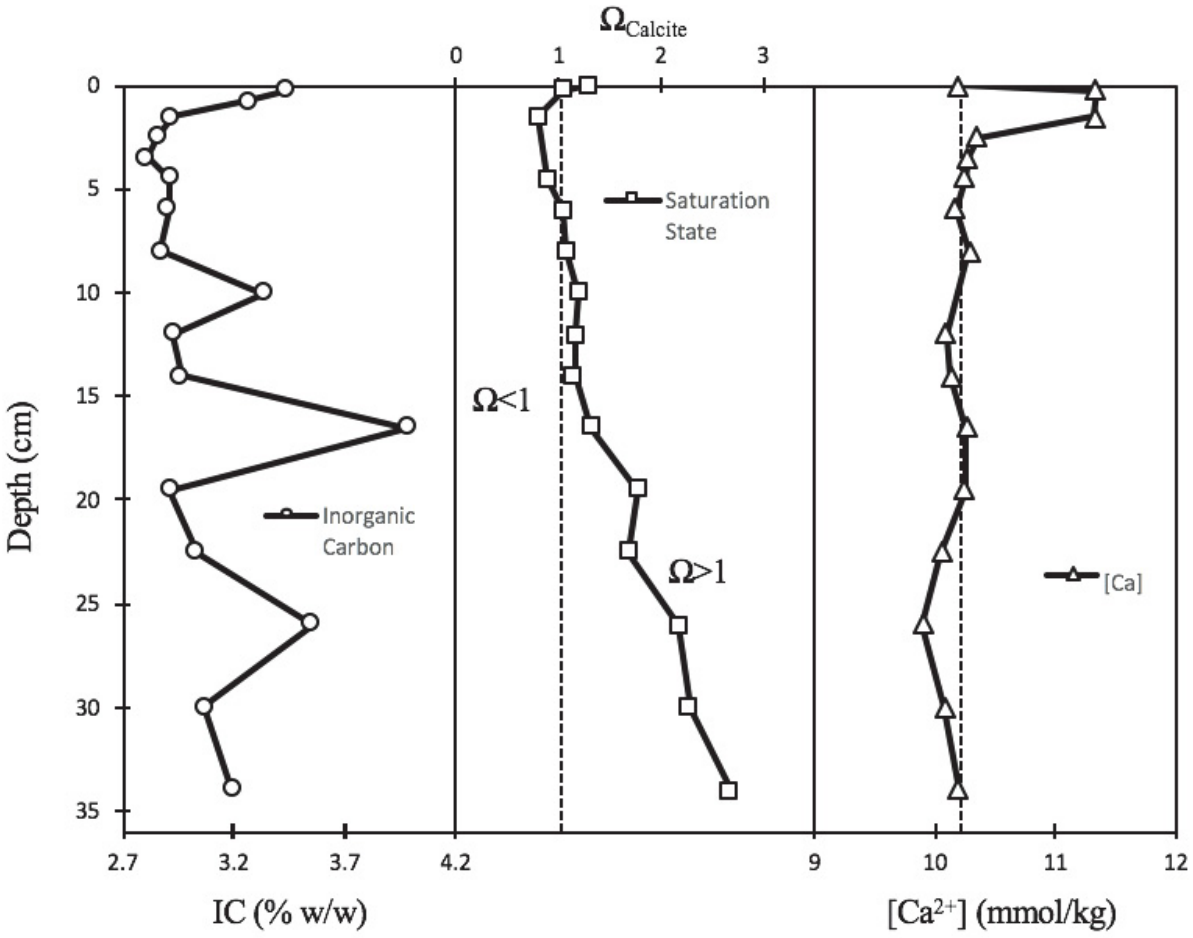

Figure 2.4: Inorganic carbon (IC) content and pore water calcite saturation state and $[Ca^{2+}]$ vertical profiles at Station Anticosti (2017). The amount of $CaCO_3$ lost to dissolution was calculated from the IC profile (to 8cm depth, 1x1x8cm) to be 19.4 µmol/cm^2.

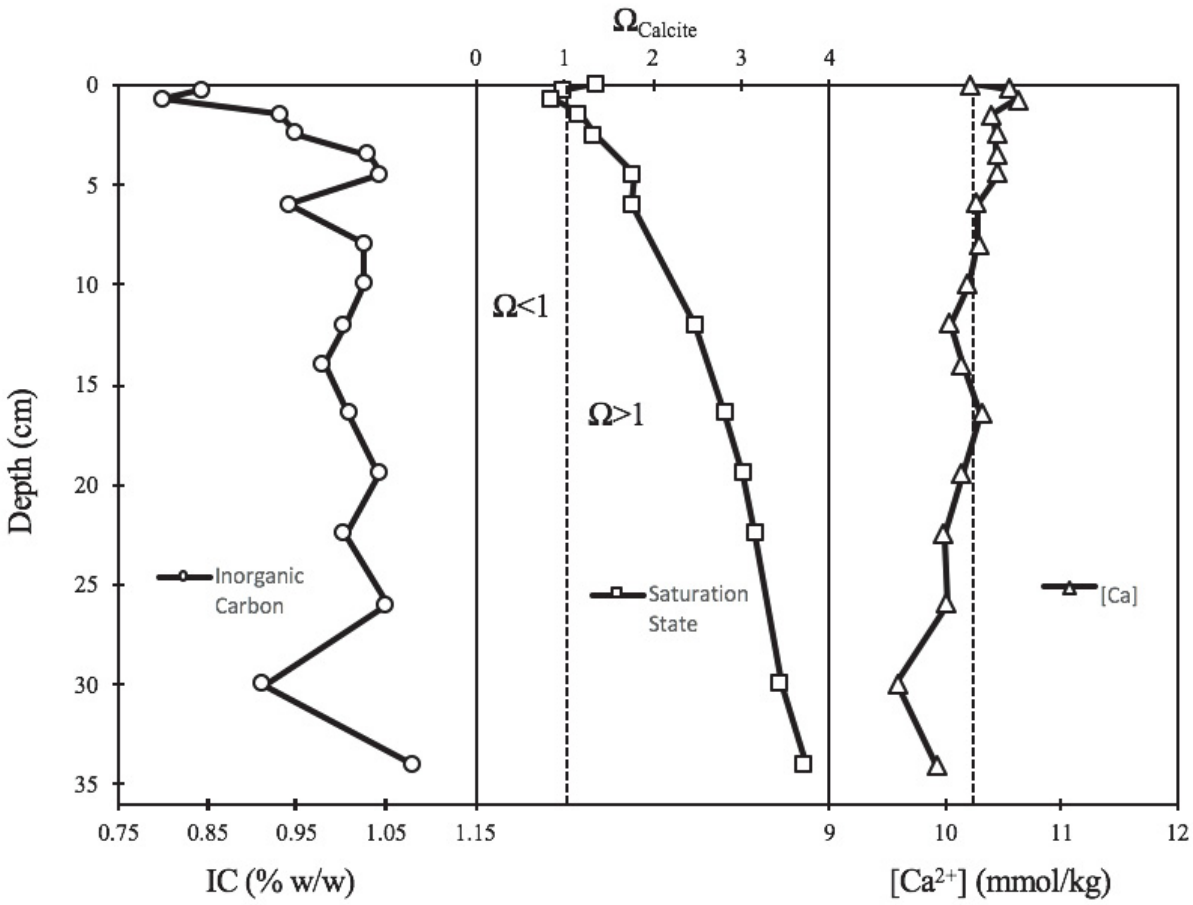

Figure 2.5: Inorganic carbon (IC) content and pore water calcite saturation state and [Ca^{2+}] vertical profiles at Station 18 (2016).

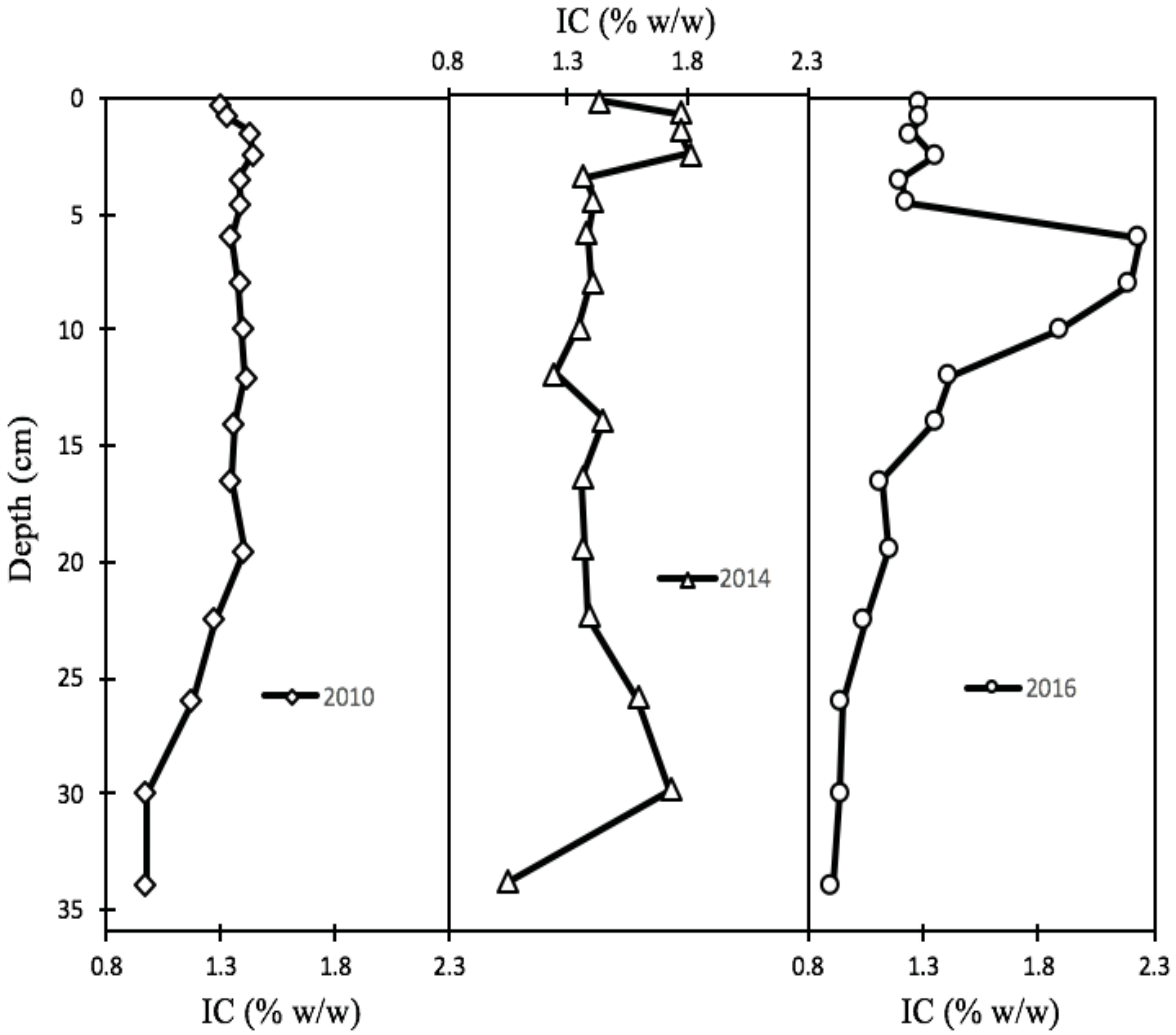

Figure 2.6: Inorganic carbon (IC) vertical profiles of Station 17 for the years 2010, 2014 and 2016. Large subsurface deviations in the 2014 and 2016 cores are likely due to the presence of adventitious shells (molluscs) or large $CaCO_3$ hard parts.

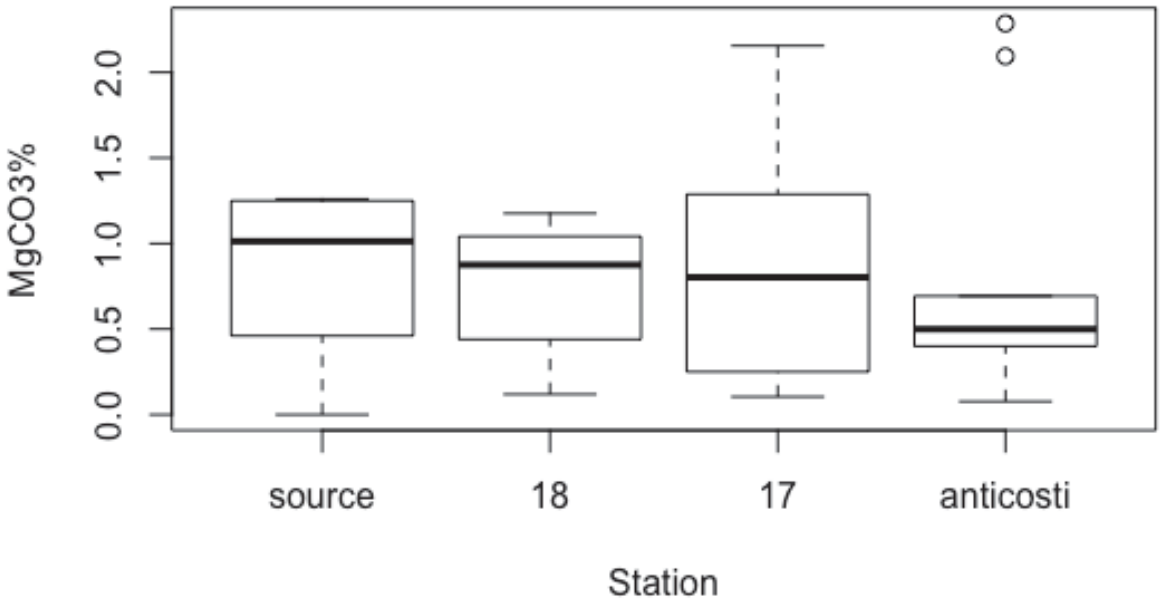

Figure 2.7: Box plots comparing the range of mol% $MgCO_3$ of the source carbonate rock and the detrital carbonates within the Laurentian Trough sediments near Anticosti Island.

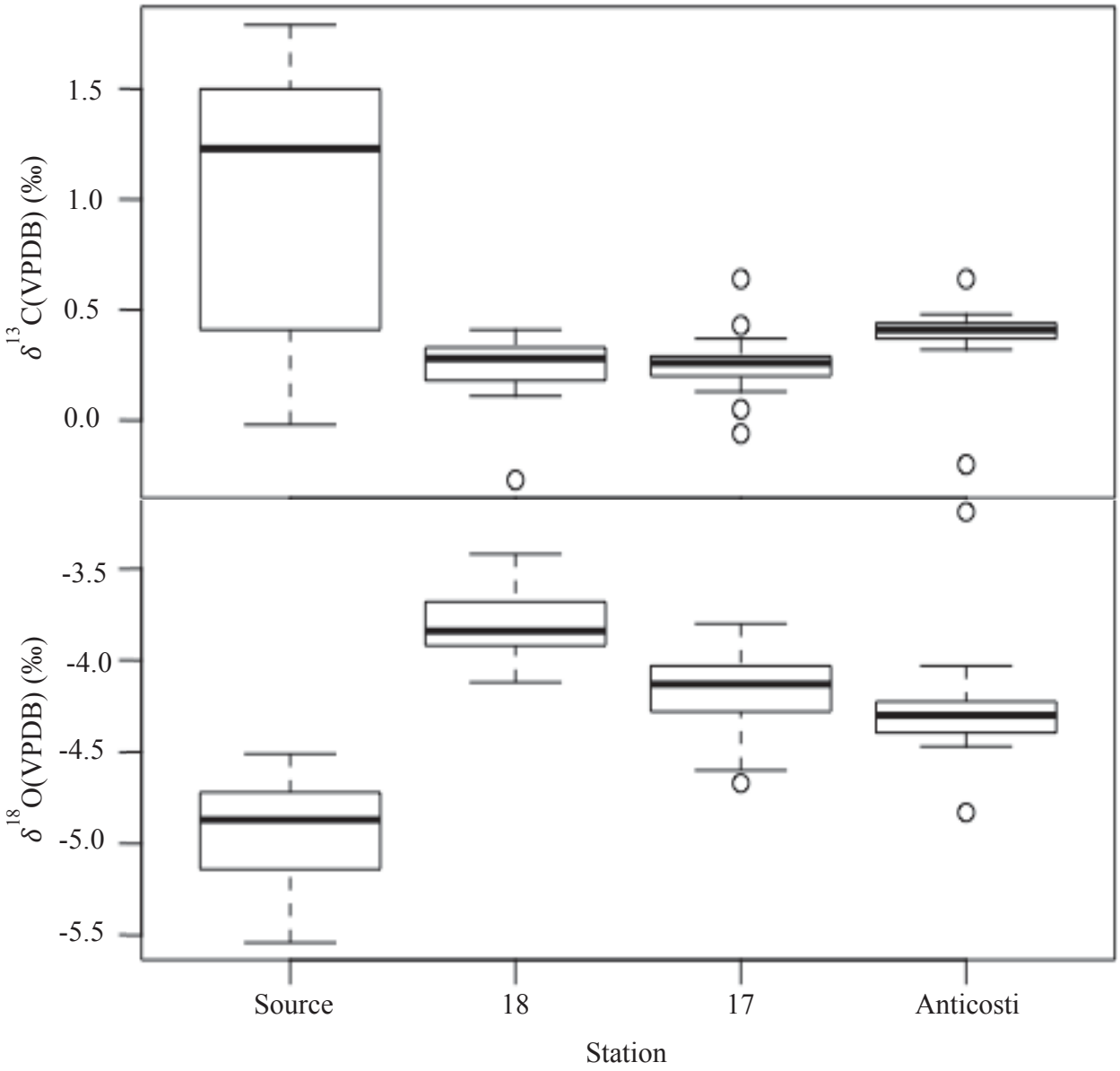

Figure 2.8: Box plots showing the difference between the stable carbon and oxygen isotope signatures of the source carbonate rock and the detrital carbonates within the Laurentian Trough sediments near Anticosti Island.

Table 2.1: Location of sample sites and selected characteristics of overlying waters (OLW).

Station	**Month/Year**	**Location**	**Depth (m)**	**T (C°)**	**S_P**	**pH_T (OLW)**	**$\Omega_{Calcite}$ (OLW)**
18	July 2003	49°16.056'N 64°15.946'W	391	5.5	34.775	7.88 (2006)	1.83 (2006)
17	July 2010	48°58.0'N 63°07.0'W	404	5.17	34.751	7.801	1.46
18	June 2013	49°15.4'N 64°15.9' W	376	5.6	34.72	7.718	1.27
17	September 2014	48°58.01'N 63°06.99'W	406	5.7	34.81	7.829	1.62
18	May 2016	49°15.70'N 64°15.69'W	381	6.02	34.777	7.739	1.36
17	May 2016	48°58.15'N 63°07.32'W	401	5.99	34.785	7.758	1.48
Anticosti	June 2017	49°21.19'N 63°56.97'W	337	6.08	34.72	7.701	1.29

Table 2.2a-g: Master Data Sheet

a) Station 18 (2003)

Depth (cm)	Porosity	IC (weight %)	OC (weight %)	$\delta^{13}C(IC)$ (‰ vs PDB)	$\delta^{18}O(IC)$ (‰ vs PDB)	$\delta^{13}C(DIC)$ (‰ vs PDB)	[Mn] (µmol/kg (SW))	[Fe] (µmol/kg (SW))	[Ca] (mmol/kg (SW))	SRP (µmol/kg (SW))	TA (µmol/kg (SW))	DIC (µmol/kg (SW))	pH_T	$\Omega_{Calcite}$
0.0-0.5	0.90	0.92	1.79											
0.5-1.0	0.88	0.98	1.75											
1.0-2.0	0.87	1.05	1.72											
2.0-3.0	0.85	1.12	1.71											
3.0-4.0	0.84	1.05	1.73											
4.0-5.0	0.83	1.09	1.66											
5.0-7.0	0.85	1.07	1.58											
7.0-10.0	0.81	1.04	1.61											
10.0-13.0	0.82	1.02	1.57											
13.0-16.0	0.81	1.08	1.56											
16.0-20.0	0.81	1.05	1.52											
20.0-25.0	0.82	1.06	1.49											
25.0-30.0	0.81	1.09												
30.0-35.0	0.81	1.11												

b) Station 18 (2013)

Depth (cm)	Porosity	IC (weight %)	OC (weight %)	$\delta^{13}C(IC)$ (‰ vs PDB)	$\delta^{18}O(IC)$ (‰ vs PDB)	$\delta^{13}C(DIC)$ (‰ vs PDB)	[Mn] (µmol/kg (SW))	[Fe] (µmol/kg (SW))	[Ca] (mmol/kg (SW))	SRP (µmol/kg (SW))	TA (µmol/kg (SW))	DIC (µmol/kg (SW))	pH_T	$\Omega_{Calcite}$
O.L.W.													7.72	1.27
0.0-0.5	0.90	0.95	1.65				0.00	0.00						
0.5-1.0	0.90	0.90	1.63				0.00	0.00						
1.0-2.0	0.82	0.91	1.67				7.10	0.00						
2.0-3.0	0.87	0.98	1.64				7.81	0.00						
3.0-4.0	0.86	1.00	1.60				25.32	0.00						
4.0-5.0	0.85	1.00	1.62				131.80	0.00						
5.0-7.0	0.83	1.07	1.51				141.50	0.00						
7.0-9.0	0.82	1.06	1.56				129.20	24.68						
9.0-11.0	0.82	1.05	1.60				165.64	23.05						
11.0-13.0	0.81	1.04	1.54				191.67	10.94						
13.0-15.0	0.81	1.06	1.47				213.68	5.12						
15.0-18.0	0.81	1.03	1.50				207.52	14.43						
18.0-21.0	0.80	1.05	1.40				185.28	5.82						
21.0-24.0	0.81	1.05	1.49				150.73	6.52						
24.0-28.0	0.82	1.06	1.48				130.62	0.00						
28.0-32.0	0.82	1.05	1.47				102.46	0.00						
32.0-36.0	0.81	1.10	1.42				84.71	0.00						

c) Station 18 (2016)

Depth (cm)	Porosity	IC (weight %)	OC (weight %)	$\delta^{13}C(IC)$ (‰ vs PDB)	$\delta^{18}O(IC)$ (‰ vs PDB)	$\delta^{13}C(DIC)$ (‰ vs PDB)	[Mn] (µmol/kg (SW))	[Fe] (µmol/kg (SW))	[Ca] (mmol/kg (SW))	SRP (µmol/kg (SW))	TA (µmol/kg (SW))	DIC (µmol/kg (SW))	pH_T	$\Omega_{Calcite}$
O.L.W.						-0.09			10.21	~2.2	2316.00		7.74	1.36
0.0-0.5	0.91	0.84	1.70	-0.27	-3.80	-1.46		2.64	10.56	5.81	2441.00		7.58	1.00
0.5-1.0	0.90	0.80	1.66	0.15	-4.11	-1.66			10.62	13.16	2530.80		7.49	0.87
1.0-2.0	0.88	0.93	1.73	0.11	-4.12	-1.90	47.91	2.45	10.40	11.31	2603.73		7.62	1.17
2.0-3.0	0.87	0.95	1.64	0.23	-3.62	-2.26	139.82	2.79	10.44	12.99	2675.84		7.67	1.34
3.0-4.0	0.84	1.03	1.56	0.22	-4.03		104.98	2.55	10.44	16.75				
4.0-5.0	0.84	1.04	1.54	0.31	-3.86	-2.96	115.22	7.52	10.45	14.36	2785.12		7.78	1.78
5.0-7.0	0.83	0.94	1.72	0.18	-3.98	-2.93	108.35	17.20	10.27	16.35	2766.92		7.78	1.77
7.0-9.0	0.82	1.03	1.55	0.24	-3.89	-4.07	115.66	37.15	10.28	20.61	2897.39			
9.0-11.0	0.81	1.02	1.53	0.41	-3.84	-4.88	125.97	19.56	10.19	14.31	3155.29			
11.0-13.0	0.81	1.00	1.58	0.32	-3.92	-6.54	141.89	15.37	10.04	14.56	3476.69		7.83	2.47
13.0-15.0	0.81	0.98	1.57	0.30	-3.88	-6.85	141.53	6.54	10.14	14.67	3770.25			
15.0-18.0	0.81	1.01	1.50	0.17	-3.42	-7.61	141.60	13.54	10.30	23.17	4045.94		7.82	2.83
18.0-21.0	0.81	1.04	1.47	0.34	-3.78	-8.43	141.73	7.71	10.14	25.03	4327.94		7.82	3.03
21.0-24.0	0.80	1.00	1.48	0.39	-3.68	-9.47	134.74	7.61	9.99	30.33	4788.40		7.79	3.16
24.0-28.0	0.81	1.05	1.39	0.33	-3.80	-10.40	125.53	3.36	10.01	31.60	5302.21			
28.0-32.0	0.81	0.91	1.57	0.33	-3.66	-11.05	105.85	2.42	9.59	33.91	5537.97		7.77	3.46
32.0-36.0	0.81	1.08	1.44	0.28	-3.54	-11.34	86.41	2.54	9.91	53.66	5782.74		7.78	3.72

d) Station 17 (2010)

Depth (cm)	Porosity	IC (weight %)	OC (weight %)	$\delta^{13}C(IC)$ (‰ vs PDB)	$\delta^{18}O(IC)$ (‰ vs PDB)	$\delta^{13}C(DIC)$ (‰ vs PDB)	[Mn] (µmol/kg (SW))	[Fe] (µmol/kg (SW))	[Ca] (mmol/kg (SW))	SRP (µmol/kg (SW))	TA (µmol/kg (SW))	DIC (µmol/kg (SW))	pH_T	$\Omega_{Calcite}$
O.L.W.													7.80	1.46
0.0-0.5	0.90	1.30	1.58											
0.5-1.0	0.89	1.33	1.60											
1.0-2.0	0.85	1.43	1.59											
2.0-3.0	0.83	1.43	1.54											
3.0-4.0	0.81	1.38	1.40											
4.0-5.0	0.80	1.38	1.43											
5.0-7.0	0.80	1.34	1.42											
7.0-9.0	0.79	1.38	1.39											
9.0-11.0	0.79	1.39	1.25											
11.0-13.0	0.80	1.40	1.24											

Table 2.2a-g: Master Data Sheet (cont)

13.0-15.0	0.79	1.36	1.43												
15.0-18.0	0.79	1.35	1.28												
18.0-21.0	0.77	1.40	1.00												
21.0-24.0	0.81	1.27	1.09												
24.0-28.0	0.79	1.17	0.68												
28.0-32.0	0.77	0.97	0.54												
32.0-36.0	0.77	0.97	0.55												

e) Station 17 (2014)

Depth (cm)	Porosity	IC (weight %)	OC (weight %)	$\delta^{13}C(IC)$ (‰ vs PDB)	$\delta^{18}O(IC)$ (‰ vs PDB)	$\delta^{13}C(DIC)$ (‰ vs PDB)	[Mn] (µmol/kg (SW))	[Fe] (µmol/kg (SW))	[Ca] (mmol/kg (SW))	SRP (µmol/kg (SW))	TA (µmol/kg (SW))	DIC (µmol/kg (SW))	pH_T	$\Omega_{Calcite}$
O.L.W.									10.22				7.83	1.62
0.0-0.5	0.88	1.43	1.58						10.10			2462.22		
0.5-1.0	0.88	1.77	1.60									2520.26		
1.0-2.0	0.87	1.77	1.59						10.02			2583.88		
2.0-3.0	0.85	1.81	1.54				28.52	3.25	9.99			2575.10		
3.0-4.0	0.81	1.37	1.40				48.00	7.85	9.85			2622.47		
4.0-5.0	0.80	1.41	1.43				45.87	7.97	9.74			2641.62		
5.0-7.0	0.80	1.38	1.42				33.50	9.29	9.83			2700.68		
7.0-9.0	0.79	1.40	1.39				38.68	9.87	9.54			2699.82		
9.0-11.0	0.79	1.35	1.25				36.20	13.18	9.64			2732.84		
11.0-13.0	0.77	1.25	1.24				36.89	11.39	9.72			2792.76		
13.0-15.0	0.79	1.45	1.43				35.65	5.03	9.93			2835.40		
15.0-18.0	0.78	1.36	1.28				34.58	7.01	9.75			2864.49		
18.0-21.0	0.79	1.37	1.00				35.15	8.77	9.87			2916.54		
21.0-24.0	0.78	1.39	1.09				35.42	6.89	9.82			2985.16		
24.0-28.0	0.78	1.59	0.68				36.11	6.17	9.69			3053.39		
28.0-32.0	0.78	1.73	0.54				35.18	9.92	9.77			3118.39		
32.0-36.0	0.79	1.05	0.55											

f) Station 17 (2016)

Depth (cm)	Porosity	IC (weight %)	OC (weight %)	$\delta^{13}C(IC)$ (‰ vs PDB)	$\delta^{18}O(IC)$ (‰ vs PDB)	$\delta^{13}C(DIC)$ (‰ vs PDB)	[Mn] (µmol/kg (SW))	[Fe] (µmol/kg (SW))	[Ca] (mmol/kg (SW))	SRP (µmol/kg (SW))	TA (µmol/kg (SW))	DIC (µmol/kg (SW))	pH_T	$\Omega_{Calcite}$
O.L.W.													7.76	1.48
0.0-0.5	0.82	1.28	1.64	0.05	-4.21									
0.5-1.0	0.81	1.29	1.55	0.43	-4.19									
1.0-2.0	0.79	1.24	1.64	0.21	-4.04									
2.0-3.0	0.79	1.35	1.72	0.19	-4.13									
3.0-4.0	0.79	1.20	1.56	0.26	-4.04									
4.0-5.0	0.78	1.23	1.56	0.28	-3.84									
5.0-7.0	0.77	2.24	1.20	-0.06	-4.28									
7.0-9.0	0.77	2.19	0.78	0.31	-4.00									
9.0-11.0	0.76	1.89	1.02	0.64	-4.15									
11.0-13.0	0.78	1.41	1.25	0.23	-4.08									
13.0-15.0	0.78	1.35	1.21	0.27	-3.98									
15.0-18.0	0.78	1.12	1.31	0.29	-4.03									
18.0-21.0	0.75	1.15	1.07	0.37	-3.80									
21.0-24.0	0.77	1.04	0.66	0.27	-4.38									
24.0-28.0	0.77	0.95	0.68	0.13	-4.60									
28.0-32.0	0.78	0.94	0.61	0.21	-4.67									
32.0-36.0	0.79	0.90	0.72	0.20	-4.34									

g) Station Anticosti (2017)

Depth (cm)	Porosity	IC (weight %)	OC (weight %)	$\delta^{13}C(IC)$ (‰ vs PDB)	$\delta^{18}O(IC)$ (‰ vs PDB)	$\delta^{13}C(DIC)$ (‰ vs PDB)	[Mn] (µmol/kg (SW))	[Fe] (µmol/kg (SW))	[Ca] (mmol/kg (SW))	SRP (µmol/kg (SW))	TA (µmol/kg (SW))	DIC (µmol/kg (SW))	pH_T	$\Omega_{Calcite}$
O.L.W.						-0.29			10.20	~1.8	2307.96		7.70	1.29
0.0-0.5	0.88	3.44	0.80	0.34	-4.32	-1.31	23.72	3.15	11.33	3.38	2480.05	2339.54	7.58	1.04
0.5-1.0	0.86	3.26	1.05	0.40	-4.37	-1.59	56.98	3.60		6.13	2447.78	2363.82	7.57	1.25
1.0-2.0	0.84	2.92	1.47	0.42	-4.38	-2.06	51.07	25.34	11.32	8.28	2422.45	2397.26	7.46	0.81
2.0-3.0	0.83	2.85	1.49	0.44	-4.03	-2.26	56.90	51.38	10.35	12.64				
3.0-4.0	0.81	2.81	1.61	0.38	-4.30	-2.14	85.60	37.03	10.27	12.95	2590.28	2471.36	7.57	1.08
4.0-5.0	0.79	2.91	1.52	0.41	-4.29	-2.74	93.15	33.50	10.25	13.14	2672.56	2628.88	7.47	0.90
5.0-7.0	0.80	2.91	1.52	0.38	-4.20	-2.59	74.57	24.13	10.17	10.72	2613.53	2598.02	7.54	1.06
7.0-9.0	0.79	2.87	1.53	0.44	-4.24	-3.56	70.26	32.83	10.28	12.07	2766.47	2782.21	7.51	1.08
9.0-11.0	0.79	3.33	1.07	0.44	-4.43	-4.03	59.09	21.78		13.86	2789.17	2841.42	7.57	1.21
11.0-13.0	0.78	2.93	1.43	0.41	-4.17	-4.30	59.14	20.33	10.10	22.88	3037.65	2969.11	7.56	1.18
13.0-15.0	0.78	2.96	1.43	0.48	-4.29	-5.27	75.34	18.29	10.13	29.27	3135.44	3131.00	7.55	1.15
15.0-18.0	0.77	3.98	0.33	0.42	-4.21	-5.23	69.06	16.18	10.26	22.95	3128.96	3145.96	7.57	1.33
18.0-21.0	0.76	2.91	1.50	0.44	-4.25	-5.14	44.97	6.60	10.25	21.24	3264.00	3101.68	7.69	1.79
21.0-24.0	0.76	3.03	1.36	0.36	-4.47	-5.76	38.05	6.97	10.05	21.11		3231.22	7.64	1.69
24.0-28.0	0.77	3.55	0.83	0.35	-4.41	-5.76	27.21	4.40	9.89	15.52	3353.81	3139.52	7.75	2.17
28.0-32.0	0.77	3.07	1.36	0.32	-4.43	-6.07	23.74	4.22	10.07	15.74	3180.21	3258.05	7.75	2.29
32.0-36.0	0.77	3.19	1.27	0.38	-4.31	-5.99	19.80	5.37	10.20	14.53	3178.87	3270.88	7.69	2.68

Table 2.3: Sequence of diagenetic reactions in marine sediments and the corresponding effects on Carbonate Alkalinity (A_C), pH and saturation state (Ω_C).

		ΔA_C	pH	Ω
Aerobic Respiration	$(CH_2O)_{106}(NH_3)_{16}H_3PO_4 + 138O_2 \longrightarrow 106HCO_3^- + 16NO_3^- + HPO_4^{2-} + 16H_2O + 124H^+$	-	-	-
Denitrification	$(CH_2O)_{106}(NH_3)_{16}H_3PO_4 + 94.4NO_3^- \longrightarrow 106HCO_3^- + 55.2N_2 + HPO_4^{2-} + 71.2H_2O + 13.6H^+$	+	-	-
Manganese Reduction	$(CH_2O)_{106}(NH_3)_{16}H_3PO_4 + 236MnO_2 + 364H^+ \longrightarrow 106HCO_3^- + 236Mn^{2+} + 8N_2 + HPO_4^{2-} + 260H_2O$	+	+	+
Iron Reduction	$(CH_2O)_{106}(NH_3)_{16}H_3PO_4 + 424Fe(OH)_3 + 759H^+ \longrightarrow 106HCO_3^- + 424Fe^{2+} + 16NH_4^+ + HPO_4^{2-} + 1060H_2O$	+	+	+
Sulfate Reduction	$(CH_2O)_{106}(NH_3)_{16}H_3PO_4 + 53SO_4^{2-} \longrightarrow 106HCO_3^- + 53HS^- + 16NH_4^+ + HPO_4^{2-} + 39H^+$	+	-	+

2.8 – References

Ahm, A. S. C., Bjerrum, C. J., Blättler, C. L., Swart, P. K., & Higgins, J. A. (2018). Quantifying early marine diagenesis in shallow-water carbonate sediments. Geochimica et Cosmochimica Acta. doi:10.1016/j.gca.2018.02.042

Archer, D., Kheshgi, H., & Maier-Reimer, E. (1998). Dynamics of fossil fuel CO_2 neutralization by marine $CaCO_3$. Global Biogeochemical Cycles, 12(2), 259-276.

Bauer, J. E., Cai, W. J., Raymond, P. A., Bianchi, T. S., Hopkinson, C. S., & Regnier, P. A. (2013). The changing carbon cycle of the coastal ocean. Nature, 504(7478), 61-70. 10.1038/nature12857.

Berner, R. A., & Morse, J. W. (1974). Dissolution kinetics of calcium carbonate in sea water; IV, Theory of calcite dissolution. American Journal of Science, 274(2), 108-134.

Berner, E., & Berner, R. (1996). Global environment water, air, and geochemical cycles Prentice-Hall. Englewood Cliffs, New Jersey, 488p.

Bickert T. (2006) Influence of Geochemical Processes on Stable Isotope Distribution in Marine Sediments. In: Schulz H.D., Zabel M. (Eds.) Marine Geochemistry, 339-369. Springer, Berlin, Heidelberg.

Bischoff, W. D., Bishop, F. C., & Mackenzie, F. T. (1983). Biogenically produced magnesian calcite: inhomogeneities in chemical and physical properties; comparison with synthetic phases. American Mineralogist, 68(11-12), 1183-1188.

Boudreau, B. P., Canfeld, D. E., & Mucci, A. (1992). Early diagenesis in a marine sapropel, Mangrove Lake, Bermuda. Limnology and Oceanography, 37(8), 1738-1753.

Cai, W.J., Hu, X., Huang, W.J., Murrell, M.C., Lehrter, J.C., Lohrenz, S.E., Chou, W.C., Zhai, W., Hollibaugh, J.T., Wang, Y. and Zhao, P. (2011). Acidification of subsurface coastal waters enhanced by eutrophication. Nature Geoscience, 4, 766–770.

Caldeira, K., & Wickett, M. E. (2005). Ocean model predictions of chemistry changes from carbon dioxide emissions to the atmosphere and ocean. Journal of Geophysical Research, Oceans, 110(C9), doi:10.1029/2004JC002671.

Clayton, T. D., & Byrne, R. H. (1993). Spectrophotometric seawater pH measurements: total hydrogen ion concentration scale calibration of m-cresol purple and at-sea results. Deep-Sea Research Part I: Oceanographic Research Papers, 40(10), 2115-2129.

Desrochers, A. (2006). Rocky shoreline deposits in the lower Silurian (upper Llandovery, Telychian) Chicotte formation, Anticosti Island, Quebec. Canadian Journal of Earth Sciences, 43(8), 1205-1214.

Desrochers, A., Farley, C., Achab, A., Asselin, E., & Riva, J. F. (2010). A far-field record of the end Ordovician glaciation: the Ellis Bay Formation, Anticosti Island, Eastern Canada. Palaeogeography, Palaeoclimatology, Palaeoecology, 296(3), 248-263.

Dickson, A. G., & Millero, F. J. (1987). A comparison of the equilibrium constants for the dissociation of carbonic acid in seawater media. Deep Sea Research Part A. Oceanographic Research Papers, 34(10), 1733-1743.

Dickson, A. G. (1990). Thermodynamics of the dissociation of boric acid in synthetic seawater from 273.15 to 318.15 K. Deep Sea Research Part A. Oceanographic Research Papers, 37(5), 755-766.

Doney, S. C., Fabry, V. J., Feely, R. A., & Kleypas, J. A. (2009). Ocean acidification: the other CO_2 problem, Annual Review in Marine Sciences, 1: 169-192. doi:10.1146/annurev.marine.010908.163834

Edenborn, H.M., Mucci, A., Belzile, N., Lebel, J., Silverberg N. & Sundby, B. (1986). A glove box for the fine-scale subsampling of sediment box cores. Sedimentology, 33, 147-150.

Feely, R. A., Sabine, C. L., Lee, K., Berelson, W., Kleypas, J., Fabry, V. J., & Millero, F. J. (2004). Impact of anthropogenic CO_2 on the $CaCO_3$ system in the oceans. Science, 305(5682), 362-366.

Feely, R. A., Doney, S. C., & Cooley, S. R. (2009). Ocean acidification: Present conditions and future changes in a high-CO_2 world. Oceanography, 22(4), 36-47.

Froelich, P., Klinkhammer, G. P., Bender, M. L., Luedtke, N. A., Heath, G. R., Cullen, D., Dauphin, P., Hammond, D., Hartman, B., & Maynard, V. (1979). Early oxidation of organic matter in pelagic sediments of the eastern equatorial Atlantic: suboxic diagenesis. Geochimica et Cosmochimica Acta, 43(7), 1075-1090.

Gaillard, J. F., Pauwels, H., & Michard, G. (1989). Chemical diagenesis in coastal marine-sediments. Oceanologica Acta, 12(3), 175-187.

Gattuso, J. P., Frankignoulle, M., & Wollast, R. (1998). Carbon and carbonate metabolism in coastal aquatic ecosystems. Annual Review of Ecology and Systematics, 29(1), 405-434.

Gattuso, J. P., & Hansson, L. (2011). Ocean acidification: background and history. In: Gattuso, J.P., & Hansson, L. (Ed.), Ocean Acidification, 1-20. Oxford University Press, New York.

Gehlen, M., Gruber, N., Gangstø, R., Bopp, L., & Oschlies, A. (2011). Biogeochemical consequences of ocean acidification and feedbacks to the earth system. In: Gattuso, J.P., & Hansson, L. (Ed.), Ocean Acidification, 230-248. Oxford University Press, New York.

Genovesi, L., sde Vernal, A., Thibodeau, B., Hillaire-Marcel, C., Mucci, A., & Gilbert, D. (2011). Recent changes in bottom water oxygenation and temperature in the Gulf of St. Lawrence: Micropaleontological and geochemical evidence. Limnology and Oceanography, 56(4), 1319-1329.

Gilbert, D., Sundby, B., Gobeil, C., Mucci, A., & Tremblay, G. H. (2005). A seventy-two-year record of diminishing deep-water oxygen in the St. Lawrence Estuary: The northwest Atlantic connection. Limnology and Oceanography, 50(5), 1654-1666.

Grasshoff, K., Kremling, K. & Ehrhardt, M. (1999). Methods of Seawater Analysis, 3, Weinheim, Germany: Wiley-VCH.

IPCC. (2007). Climate change 2007: the scientific basis. Contribution of Working Group I to the Fourth Assessment Report of the Intergovernmental Panel on Climate Change. Cambridge University Press, New York.

Jaegle M. (2015). Nature et origine des sédiments de surface de l'estuaire du Saint-Laurent. M.Sc. thesis, Université du Québec à Rimouski, Rimouski, Québec.

James, N. P., Desrochers, A., & Kyser, T. K. (2015). Polygenetic (Polyphase) karsted hardground omission surfaces In: Lower Silurian Neritic Limestones: Anticosti Island, Eastern Canada. Journal of Sedimentary Research, 85(9), 1138-1154.

Kim, S. T., Mucci, A., & Taylor, B. E. (2007). Phosphoric acid fractionation factors for calcite and aragonite between 25 and 75 C: revisited. Chemical Geology, 246(3-4), 135-146.

Le Quéré, C., Raupach, M. R., Canadell, J. G., Marland, G., Le Quéré et al, C., Le Quéré et al, C., Raupach, M. R., Canadell, J. G., Marland, G., Bopp, L., Ciais, P., Conway, T. J., Doney, S. C., Feely, R. A., Foster, P., Friedlingstein, P., Gurney, K., Houghton, R. A., House, J. I., Huntingford, C., Levy, P. E., Lomas, M. R., Majkut, J., Metzl, N., Ometto, J. P., Peters, G. P., Prentice, I. C., Randerson, J. T., Running, S. W., Sarmiento, J. L., Schuster, U., Sitch, S., Takahashi, T., Viovy, N., van der Werf, G. R., Woodward, F. I., & et al. (2009). Trends in the sources and sinks of carbon dioxide: Nature Geoscience, 2(12), 831-836.

Lewis, E., & Wallace, D. (1998). CO2SYS Program. Carbon Dioxide Information Analysis Center, Oak Ridge National Laboratory Environmental Sciences Division, Oak Ridge, Tennessee.

Mackenzie, F. T., Andersson, A. J., Arvidson, R. S., Guidry, M. W., & Lerman, A. (2011). Land–sea carbon and nutrient fluxes and coastal ocean CO_2 exchange and acidification: Past, present, and future. Applied Geochemistry, 26, S298-S302.

Mehrbach, C., Culberson, C. H., Hawley, J. E., & Pytkowicx, R. M. (1973). Measurement of the apparent dissociation constants of carbonic acid in seawater at atmospheric pressure 1. Limnology and Oceanography, 18(6), 897-907.

Morse, J. W., Arvidson, R. S., & Lüttge, A. (2007). Calcium carbonate formation and dissolution. Chemical Reviews, 107(2), 342-381.

Mucci, A. (1983). The solubility of calcite and aragonite in seawater at various salinities, temperatures, and one atmosphere total pressure. American Journal of Science, 283(7), 780-799.

Mucci, A., Sundby, B., Gehlen, M., Arakaki, T., Zhong, S., & Silverberg, N. (2000). The fate of carbon in continental shelf sediments of eastern Canada: a case study. Deep Sea Research Part II: Topical Studies in Oceanography, 47(3), 733–760.

Mucci, A., Starr, M., Gilbert, D., & Sundby, B. (2011). Acidification of Lower St. Lawrence Estuary bottom waters. Atmosphere-Ocean, 49(3), 206–218.

Nota, D.J.G., Loring, D.H. (1964). Recent depositional conditions in the St. Lawrence River and Gulf – A reconnaissance survey. Marine Geology, 2, 198-235.

Orr, J.C., Fabry, V.J., Aumont, O., Bopp, L., Doney, S.C., Feely, R.A., Gnanadesikan, A., Gruber, N., Ishida, A., Joos, F., Key, R.M., Lindsay, K., Maier-Reimer, E., Matear, R., Monfray, P., Mouchet, A., Najjar, R.G., Plattner, G.K., Rodgers, K.B., Sabine, C.L., Sarmiento, J.L., Schlitzer, R., Slater, R.D., Totterdell, I.J., Weiring, M.F., Yamanaka, Y., & Yool, A. (2005). Anthropogenic ocean acidification over the twenty-first century and its impact on calcifying organisms. Nature, 437, 681–686.

Orr, J.C. (2011). Recent and future changes in ocean carbonate chemistry. In: Gattuso, J.P., & Hansson, L (Ed), Ocean Acidification, 41-63. Oxford University Press, New York.

Orr, J. C., Epitalon, J. M., Dickson, A. G., & Gattuso, J. P. (2018). Routine uncertainty propagation for the marine carbon dioxide system. Marine Chemistry, 207, 84-107.

Piper, D.J.W., Mudie, P.J., Fader, G.B., Josenhans, H.W., MacLean, B., Vilks, G. (1990). Quaternary geology, Chapter 10. In: Keen, M.J., Williams, G.L. (Eds.), Geology of the Continental Margin of Eastern Canada. Geological Survey of Canada, pp. 475–607.

Reeburgh, W. S. (1967). An improved interstitial water sampler1. Limnology and Oceanography, 12(1), 163-165.

Reddy, M. M. (1977). Crystallization of calcium carbonate in the presence of trace concentrations of phosphorus-containing anions. Journal of Crystal Growth, 41, 287-295.

Redfield, A. C., Ketchum, B. H., & Richards, F. A. (1963). The influence of organisms on the composition of seawater. In: Hill, M.N. (Eds.) The composition of seawater: Comparative and descriptive oceanography. The sea: ideas and observations on progress in the study of the seas, 2, 26-77.

Sabine, C.L. & Feely, R.A. (2007). The oceanic sink for carbon dioxide. Greenhouse Gas Sinks. CABI Publishing, 31-49.

Silverberg, N., Sundby, B., Mucci, A., Zhong, S., Arakaki, T., Hall, P., Landehn, A., Tengberg, A. (2000). Remineralization of organic carbon in eastern Canadian continental margin sediments. Deep-Sea Research II, 47, 699-731.

Smith, J. N., & Schafer, C. T. (1999). Sedimentation, bioturbation, and Hg uptake in the sediments of the estuary and Gulf of St. Lawrence. Limnology and Oceanography, 44(1), 207-219.

Tans, P.P. & Keeling, R. (2016). Dr. Pieter Tans, NOAA/ESRL (www.esrl.noaa.gov/gmd/ccgg/trends/) and Dr. Ralph Keeling, Scripps Institution of Oceanography (scrippsco2.ucsd.edu/).

Titschack, J., Goetz-Neunhoeffer, F., & Neubauer, J. (2011). Magnesium quantification in calcites [(Ca, Mg) CO_3] by Rietveld-based XRD analysis: revisiting a well-established method. American Mineralogist, 96(7), 1028-1038.

Chapter 3: Summary and Conclusions

3.1 – Summary of Research

Since the onset of industrialization, the oceans have absorbed just over a quarter of the anthropogenic CO_2 emitted to the atmosphere (Feely et al., 2004; Sabine et al., 2004; Sabine and Feely, 2007; Feely et al., 2009). This has led to a decrease in the surface ocean pH by an estimated 0.1 unit, corresponding to a 30% increase in proton concentration in solution (Caldeira and Wickett, 2005). Assuming the "business-as-usual" scenario (IS92a), CO_2 concentrations will exceed 700 ppm by the end of this century, leading to a further decrease in surface ocean pH by an additional 0.3-0.4 unit. A decrease in pH of this magnitude will drastically change the speciation of Dissolved Inorganic Carbon (DIC) in seawater, lowering the carbonate ion concentration by ~50%. Consequently, this will greatly lower the saturation state of the surface ocean with respect to calcite and aragonite, reducing the capacity of calcifying organisms to precipitate their shells or exoskeletons as well as affect their preservation on the seafloor.

Since the early 1930's, the minimum dissolved oxygen (DO) concentrations in the bottom waters of the Lower St. Lawrence Estuary (LSLE) and the Gulf have decreased dramatically from 125 μmol/L in the 1930's, to values as low as 49.4 μmol/L in 2017 (Gilbert et al., 2005; Mucci et al., 2011). Gilbert et al. (2005) concluded that depleted DO concentrations are primarily the result of changing mixing ratios, on the eastern Canadian continental margin, of the two major source-water masses, the Labrador Current Water (LCW) and the North Atlantic Central Water (NACW), that flow landward along the Laurentian Channel/Trough through Cabot Strait into the Gulf of St. Lawrence and ultimately into the Lower St. Lawrence Estuary. Further depletion of the bottom-water oxygen concentration is caused by the microbially-mediated oxidation of organic matter settling from the surface through the poorly ventilated, strongly stratified water column of the Gulf and Estuary. This has led to the accumulation of metabolic CO_2 in the bottom waters, their acidification and a decrease in pH of as much as 0.3-0.4 pH unit, mimicking conditions expected for the average surface ocean by 2100.

Sediments of the Laurentian Trough a nearly devoid of $CaCO_3$, except from the seafloor around Anticosti Island where detrital carbonates accumulate. This area of the Laurentian Trough is an ideal site to study the impacts of ocean acidification on the preservation of sedimentary $CaCO_3$ minerals. To the best of our knowledge, the preservation and dissolution of carbonate minerals in these sediments has not been documented. Accordingly, this research project had three major objectives to address: (1) Determine if dissolution of detrital carbonates occurs in the Laurentian Trough sediments in response to the recent acidification of the bottom waters in the Gulf, (2) Determine if preservation of these detrital carbonates has varied over time and (3) Investigate if preservation varies spatially within the Gulf. To address these objectives, box cores were taken over the past ~15 years at three stations (17 (2010, 2014, 2016), 18 (2003, 2013, 2016) and Anticosti (2017)) in the Gulf of St. Lawrence, in the vicinity of Anticosti Island. Significant $CaCO_3$ dissolution was observed at Station 18 (2016) and Station Anticosti (2017) as the inorganic carbon content was depleted in the top 8 cm of each core. Pore water profiles confirm the active dissolution of carbonate minerals within the oxic layer of the sediment as they become undersaturated with respect to calcite ($1>\Omega_{Calcite}$) and calcium concentrations increase immediately below the sediment-water interface (SWI). The evolution of $CaCO_3$ dissolution over time was documented at Station 18 over the years 2003, 2013 and 2016. The results revealed an acceleration in the rate of dissolution within the first centimeter (oxic layer - 1x1x1cm) starting with 0.30 $\mu mol/cm^2$/year in 2003 and intensifying to 0.58 $\mu mol/cm^2$/year in 2016, equivalent to a ~93% increase in the dissolution rate over the span of 13 years. This increase in dissolution is attributed to a notable decrease in $\Omega_{Calcite}$ (1.83 to 1.36) of the Overlying Waters (OLW) at Station 18 between 2006 and 2016. Although these waters are still supersaturated with respect to calcite, the accumulation of metabolic CO_2 during oxic diagenesis generates calcite-undersaturated pore waters and triggers dissolution. The progressive acidification of the bottom waters over this time span (2006 to 2016) means that less metabolic CO_2 is required to generate undersaturated pore waters in the oxic layer of the sediment and leads to a decreased preservation of carbonate minerals at this station. Finally, we observed that preservation of $CaCO_3$ varies spatially within the Gulf. Whereas significant dissolution is observed at both Stations 18 and Anticosti, it was undetectable at Station 17. This discrepancy likely reflects the higher saturation state of the OLW at Station 17 ($\Omega_{Calcite}$ =1.48) than at the other stations (18; $\Omega_{Calcite}$ = 1.36, Anticosti; $\Omega_{Calcite}$ = 1.29), requiring more metabolic CO_2 production to generate undersaturated pore waters. Furthermore, the

sedimentation rate at Station 17 is slightly lower (0.13 cm/year) than at the other stations (18; 0.18cm/year) which, when accompanied with an overall lower sedimentary organic carbon content, accounts for a lower sediment oxidant demand and rate of oxic diagenesis and metabolic CO_2 production.

3.2 – Implications to Ocean Acidification Research

The calcium carbonate minerals that accumulate in deep-sea sediments can potentially neutralize all of the anthropogenic CO_2 transferred to the deep ocean making them its ultimate short-term sink (100-1000 years) (Archer et al., 1998). Currently, most of the surface ocean is supersaturated ($\Omega>1$) with respect to both aragonite and calcite. The anticipated drop in surface-ocean pH of 0.3-0.4 unit by the end of this century, based on the IPCC "business-as-usual" scenario, will have a profound effect on the saturation state (Ω) of the surface ocean with respect to calcium carbonate minerals. By then, most of the ocean will be undersaturated with respect to aragonite and slightly supersaturated with respect to calcite. Hence, aragonite secreting organisms such as pteropods and corals may no longer be able to grow and may become extinct. Coincidentally, these environmental conditions are mirrored by those found in the bottom waters of the Lower St. Lawrence Estuary (Mucci et al., 2011). Therefore, the most powerful implications that can be drawn from this project is its use as a natural analogue for projected surface ocean conditions by 2100 and the fate of fossils carbonates that accumulate on shallow platforms. At a pH_T of 7.7 (Ω_C = 1.29), which correspond to the carbonate chemistry of the OLW in this study, the preservation of low magnesium calcite in sediments is greatly diminished as significant dissolution was observed in the sediments at two of the three sites investigated in this study. The time series at Station 18 displayed a large decrease in the saturation state of the OLW between 2006 and 2016, from Ω_C =1.83 to 1.36. This has caused a significant decrease in $CaCO_3$ preservation in the oxic layer (first cm) of the sediment as well as an increase in its rate of dissolution. Given that low magnesium calcite is the least soluble (i.e., most stable) calcium carbonate polymorph, high magnesium calcites and aragonite would be more susceptible to dissolution. Morse et al. (2006) dubbed high magnesium calcites (>12 mol% $MgCO_3$) that accumulate in shallow-water deposits (e.g., carbonate platforms) as the "first responders" to ocean acidification due to their higher solubility, which even exceeds that of aragonite. Thus, high

magnesium calcites will dissolve first in a sequence of decreasing $MgCO_3$ content (until 12 mol%), followed by aragonite and lastly by low magnesium calcites. Furthermore, a decrease in the surface-ocean pH, of the magnitude anticipated by the end of this century, would lower the average $MgCO_3$ content of calcites accumulating on shelves and decrease the overall abundance of aragonite (Morse et al., 2006). This, ultimately, would be detrimental to a variety of marine calcifiers (pteropods, foraminifera, gastropods, etc.) (Fabry et al., 2008; Doney et al., 2009). Many of these organisms are keystone species, lying at the base of the marine food web or play an integral role in its function, making this an issue of grave ecological importance. The fate of these biocalcifiers, however, is highly species dependent, as some organisms may adapt while others perish (Doney et al., 2009).

3.3 – Future Directions and Final Remarks

The results of this project have provided a framework for future studies of the CO_2-H_2O-$CaCO_3$ system in the Gulf of St. Lawrence and other marine environments subjected to intensified acidification by characterizing the extent of carbonate dissolution on both a spatial and temporal scale. Future work should include data collection (pH, pCO_2, DIC, TA) on a decadal scale to characterize the evolution of the carbonate system. This provide future researchers with a record of the evolution of acidification within the Gulf, as was done by Mucci et al. (2011) in the Lower St. Lawrence Estuary. Dissolution of detrital carbonates accumulating in sediments at Station 17 is not yet detectable, but will likely develop within the near future as pH decreases further in the bottom waters of the Gulf. Therefore, Station 17 is a site of particular interest for which both sediment and pore water chemistry should be monitored in time. Another interesting direction would be to core along a transect between Station 18 and Station 17 to determine the extent of $CaCO_3$ dissolution as one moves seaward in the Gulf and bottom-water saturation states progressively decrease. Monitoring of Stations 18 and Anticosti should be continued, as over the past decade the preservation of $CaCO_3$ has decreased notably and accelerated. Variation of $\partial^{13}C$ between pore water DIC and the solid phase IC were observed in this study, suggesting that contributions to pore water DIC originate from both OM degradation and IC dissolution. However, without the elaboration of a diagenetic model, such as presented in Gehlen et al. (1999), the relative contributions of these two processes to the pore water DIC pool cannot be differentiated. An

estimate of the DIC contributed from $CaCO_3$ dissolution, in conjunction with pore water calcium concentration profiles could further constrain the magnitude of dissolution within the core.

3.4 – References

Archer, D., Kheshgi, H., & Maier-Reimer, E. (1998). Dynamics of fossil fuel CO_2 neutralization by marine $CaCO_3$. Global Biogeochemical Cycles, 12(2), 259-276.

Caldeira, K., & Wickett, M. E. (2005). Ocean model predictions of chemistry changes from carbon dioxide emissions to the atmosphere and ocean. Journal of Geophysical Research, Oceans, 110(C9), doi:10.1029/2004JC002671.

Doney, S. C., Fabry, V. J., Feely, R. A., & Kleypas, J. A. (2009). Ocean acidification: the other CO_2 problem, Annual Review of Marine Science, 1: 169-192. doi:10.1146/annurev.marine.010908.163834

Fabry, V.J., Seibel, B.A., Feely, R.A., & Orr, J.C. (2008). Impacts of ocean acidification on marine fauna and ecosystem processes. ICES Journal of Marine Science, 65, 414-432.

Feely, R. A., Sabine, C. L., Lee, K., Berelson, W., Kleypas, J., Fabry, V. J., & Millero, F. J. (2004). Impact of anthropogenic CO_2 on the $CaCO_3$ system in the oceans. Science, 305(5682), 362-366.

Feely, R. A., Doney, S. C., & Cooley, S. R. (2009). Ocean acidification: Present conditions and future changes in a high-CO_2 world. Oceanography, 22(4), 36-47.

Gehlen, M., Mucci, A., & Boudreau, B. (1999). Modelling the distribution of stable carbon isotopes in porewaters of deep-sea sediments. Geochimica et Cosmochimica Acta, 63(18), 2763.

Gilbert, D., Sundby, B., Gobeil, C., Mucci, A., & Tremblay, G. H. (2005). A seventy-two-year record of diminishing deep-water oxygen in the St. Lawrence estuary: The northwest Atlantic connection. Limnology and Oceanography, 50(5), 1654-1666.

Morse, J. W., Andersson, A. J., & Mackenzie, F. T. (2006). Initial responses of carbonate-rich shelf sediments to rising atmospheric pCO_2 and "ocean acidification": Role of high Mg-calcites. Geochimica et Cosmochimica Acta, 70(23), 5814-5830.

Mucci, A., Starr, M., Gilbert, D., & Sundby, B. (2011). Acidification of Lower St. Lawrence Estuary bottom waters. Atmosphere-Ocean, 49(3), 206–218.

Sabine, C.L., Feely, R.A., Gruber, N., Key, R.M., Lee, K., Bullister, J.L., Wanninkhof, R., Wong, C.S., Wallace, D.W., Tilbrook, B., Millero, F.J., Peng, T.H., Kozyr, A., Ono, T. & Rios, A.F. (2004). The oceanic sink for anthropogenic CO_2. Science, 305(5682), 367-71.

Sabine, C.L. & Feely, R.A. (2007). The oceanic sink for carbon dioxide. Greenhouse Gas Sinks. CABI Publishing, 31-49.